THESIS FOR THE DEGREE OF LICENTIATE OF ENGINEERING

Diurnal variation of stratospheric short-lived species

MARYAM KHOSRAVI

CHALMERS

Department of Earth and Space Sciences

CHALMERS UNIVERSITY OF TECHNOLOGY

Gothenburg, Sweden, 2012

Diurnal variation of stratospheric short-lived species
MARYAM KHOSRAVI

Cover: ClO measurement made by ASUR
(Airborne SUbmillimeter Radiometer)
on 23 January 2000 in the Arctic stratosphere (top)
and corresponding smoothed model simulation (bottom).
For detailed information see chapter 4 and paper I.

Diurnal variation of stratospheric short-lived species

Maryam Khosravi
Chalmers University of Technology
Department of Earth and Space Sciences

Abstract

The depletion of ozone in the stratosphere has a direct impact on the amount of ultraviolet radiation reaching the Earth's surface. The ozone abundance and distribution is controlled by the photo-chemical reactions and catalytic cycles involving halogens (chlorine and bromine), odd hydrogen and odd nitrogen species as well as by the atmospheric transport.

An introduction to ozone related chemistry of the stratosphere and modelling of short-lived species using photo-chemical models is presented. A one dimensional (1D) atmospheric model is used in two distinct studies: modeling of short-lived species in the Arctic lower stratosphere (paper I) and in the tropical mid to upper stratosphere (paper II).

The first part of this thesis describes the diurnal variation of chlorine monoxide, ClO, which is the most important short-lived species controlling ozone in the polar lower stratosphere during winter and early-spring. The ClO-dimer cycle, involving ClO and its nighttime reservoir Cl_2O_2, contributes to about 75% of the polar ozone loss. ClO measurements from an airborne submillimeter radiometer in the Arctic twilight have been compared with the results from a 1D photo-chemical model (MISU-1D), in order to validate the model and to test the kinetics of the reactions controlling the partitioning of chlorine species during the course of a day. The results show that cross sections leading to faster photolysis rates of Cl_2O_2 match best with the ClO observations. This is consistent with the recent version of the chemical kinetics evaluation by the Jet Propulsion Laboratory. Slower photolysis rates can not be reconciled with the observations since active chlorine higher than the total available chlorine would be required. The model reproduces higher nighttime ClO than the observations, however the nighttime ClO modelled using recent JPL recommendations of the thermal equilibrium constant agree within the uncertainty range of the observations. The sensitivity of the model to the assumed albedo and temperature are also tested. Neither the temperature nor the albedo uncertainties allow us to reconcile the model with the lower observed nighttime ClO. Moreover, it is found that the ClO-BrO cycle decreases ClO mostly around sunrise and sunset.

The second part of the thesis presents the partitioning and diurnal variation of chlorine, bromine, hydrogen, nitrogen and oxygen species in the tropics from the stratosphere to the lower mesosphere. Model results of the diurnal variation of HOCl (as one of the chlorine reservoirs), the related short-lived species ClO and HO_2 and HCl (as the main chlorine reservoir) for the tropics and three altitudes (35, 45 and 55 km) are compared with measurements from five satellite instruments. The model results generally agree with the observations both in terms of the absolute values and the differences between day and night.

Keywords: Arctic stratosphere, chlorine monoxide, tropical middle stratosphere, Arctic ClO, diurnal variation, short-lived species

List of Publications

- M. Khosravi, P. Baron, J. Urban, L. Froidevaux, A. I. Jonsson, Y. Kasai, K. Kuribayashi, C. Mitsuda, D. P. Murtagh, H. Sagawa, M. L. Santee, T. O. Sato, M. Shiotani, M. Suzuki, T. von Clarmann, K. A. Walker, S. Wang. *Diurnal variation of stratospheric HOCl, ClO and HO_2 at the equator: comparison of 1d model calculations with measurements of satellite instruments.* Atmos. Chem. Phys. Discuss., 12, 1-40, 2012. www.atmos-chem-phys-discuss.net/12/1/2012/, doi:10.5194/acpd-12-1-2012.

- A. Kleinböhl, M. Khosravi, J. Urban, T. Canty, R. J. Salawitch, G. C. Toon, H. Küllmann, and J. Notholt. *Constraints for the photolysis rate and the equilibrium constant of ClO-dimer from airborne and balloon-borne measurements of chlorine componds.* In preparation for submission to Journal of Geophysical Research.

Acknowledgments

First and foremost, I would like to thank my advisors: Dr. Joachim Urban and Prof. Donal Murtagh for their invaluable support, encouragement and discussion during this work. I wish to thank my colleagues in the Global Environmental Measurement and Modelling group for their support; Marston Johnston for help in editing this thesis, Kazutoshi Sagi for programming tips and being a very kind and excellent room mate and finally Ole Martin Christensen for the discussions and ideas. I would also like to thank everyone in the department of Earth and Space Sciences. My infinite thanks go to my kind husband Farzad for always being there for me, giving support and inspiration as well as my lovely son, Arvin, my parents and rest of my family for loving and believing in me.

Contents

Chapter 1

Introduction

The first observation of the Antarctic ozone hole in 1985 [Farman et al., 1985], followed by the discovery of the ClO-dimer catalytic cycle by Molina and Molina [1987] and the bromine and chlorine oxide catalytic cycle by McElroy et al. [1986], has brought attention to stratospheric ozone and related species. The discovery of the ozone hole over Antarctica raised the possibility of a similar phenomenon in the Arctic. This initiated various measurement and modelling studies of ozone and related species over the Arctic. Knowledge of partitioning of chlorine and bromine species and measurements of active and reservoir concentrations of chlorine and bromine compounds in the stratosphere helps us to understand the cycles and reactions which contribute to Antarctic and Arctic ozone loss. The stratospheric chlorine amount peaked in the late 1990s and has since then decreased. Despite the slow decrease of stratospheric chlorine, ozone loss in Antarctica remained stable at the level of the mid-1990s. However there is considerable year-to-year variability due to changes in temperature and dynamics. Ozone-sonde observations at the South Pole indicate that, for the majority of years since the mid-1980s, about 90% of ozone is removed at 18 km. The Arctic stratosphere, because of its warmer conditions and more unstable winter vortices, shows larger variability in spring-time ozone than Antarctica [WMO, 2010]. The largest Arctic ozone loss so far was observed in the winter 2010-2011, due to the persistent cold conditions over longer periods [Manney et al., 2011, Urban et al., 2011].

Most of the ozone is produced in the tropical middle stratosphere (at about 30–40 km). Ozone protects the whole living ecosystem by absorbing the Ultra Violet (UV) light in the solar radiation. Understanding of the mechanisms and the chemical reactions involved in ozone loss in the whole stratosphere in general and in the polar stratosphere in particular is necessary for controlling the man-made factors. The measurement of species involved in the ozone loss cycles and modelling of photo-chemical reactions provide the tools which enable the scientific community to asses these phenomena. Among the chemical species involved in ozone destruction, halogens in active form (chlorine and bromine radicals), hydrogen radicals (odd hydrogen) and nitrogen oxides (odd nitrogen) have important roles. This motivates the scientific community to monitor changes in these species, to measure the partitioning between the active and reservoir forms, and to compare measurements with models. Atmospheric models fill the gaps where the measurements can not represent a full picture of the

atmosphere and may also give us information for future projections.

The main goal of this study is to validate model calculations of stratospheric species related to ozone chemistry. Since the observations can not be performed at all locations and times and each observation has its own limitations and uncertainties arising from instrumental and retrieval errors, the comparison of measurements with models provides a tool to evaluate (examine) the measurements. In addition, since the models are built upon our knowledge about the atmospheric chemistry and physics, the comparison of models and measurements is a way to test our understanding of the atmosphere.

This thesis mainly focuses on simulations in two atmospheric regions, namely the Arctic lower stratosphere and the tropical middle stratosphere. Chapter 2 gives background information on physics and chemistry of the atmosphere and the structure of the atmospheric models. Chapter 3 looks at the diurnal variation of chlorine monoxide in the Arctic lower stratosphere and shows simulations of the enhanced chlorine and bromine conditions typical for winter and early spring. The model simulations have been compared with airborne measurements of chlorine monoxide in terms of changing concentrations between day and night. The sensitivity of the results to the kinetics of the involved reactions has also been tested. Chapter 4 discusses the diurnal variation of the chlorine reservoir HOCl and the related species, ClO, HO_2 and HCl in the stratosphere-mesosphere region (35–55 km). The partitioning of the main chemical families in this region is discussed. The summary and conclusion as well as an overview of the appended papers are given in chapter 5.

Chapter 2

Background

2.1 Physics of the atmosphere

2.1.1 Vertical structure

The atmosphere is the thin layer of gas surrounding the Earth and held in place by gravitation. The atmospheric pressure decreases approximately exponentially with height:

$$p(z) = p(z_0)exp(-\frac{z - z_0}{H}).$$ (2.1)

Here $p(z)$ and $p(z_0)$ are the pressure of the air at a given altitude (z) and at the surface (z_0). H is the atmosphere scale height which represents the decrease in pressure by $\frac{1}{e}$ with altitude. The scale height is estimated to be about 7 to 8 km in the lowest 100 km of the atmosphere. Scale height relates to temperature, T, ideal gas constant, R (8.3144 Jmol^{-1}K^{-1}), mean molar mass of the air, M, and acceleration due to gravitation, g, as

$$H = \frac{RT}{Mg}.$$ (2.2)

The density of air is related to pressure and decreases with height in the same manner as pressure. The air is considered as an ideal gas and thus obeys the ideal gas law

$$p = \rho RT = \frac{N}{V}k_BT,$$ (2.3)

where ρ is the air density, N the number density of air (the number of molecules per volume V) and k_B is Boltzmann's constant.

The layers of the atmosphere are defined according to the temperature gradients, or lapse rates as shown in Figure 2.1 for a standard atmosphere. The troposphere is characterized by decreasing temperature with height (negative lapse rate). The troposphere extends to about 17 km at the equator and to about 7 km at high latitudes. This layer contains about 90% of the atmospheric mass and is characterized by rapid vertical mixing. The tropopause is the region between the troposphere and the layer above, where the temperature is almost constant with altitude (laps rate $\leq 2\,$Kkm^{-1}).

In the next layer, the stratosphere, the vertical temperature gradient reverses. The stratosphere contains about 90% of the atmospheric ozone and heating due to the UV-photolysis of ozone explains the positive lapse rate of this layer. The stratosphere extends to about 50 km. Vertical mixing and turbulence are very small in the stratosphere. The stratosphere is characterized by very dry conditions, due to the very small tropospheric-stratospheric water exchange and little vertical mixing. The only chemical source of water in the stratosphere is the destruction of methane. The layer from about 50 to 80 km is called the mesosphere, with negative lapse rate, since the ozone concentration decreases with altitude. The air in this layer is more unstable compared to the stratosphere which causes stronger vertical mixing. The coldest temperatures in the atmosphere are found in this region of the atmosphere during polar summer. In the thermosphere, above 85 km, the temperature increases again with height and reaches maximum values due to the photolysis of nitrogen and oxygen. In this region, molecular diffusion is dominant over vertical mixing, allowing the formation of separate layers of nitrogen molecules, oxygen and hydrogen atoms [Brasseur et al., 1999, Brasseur and Solomon, 2005, Wallace and Hobbs, 2006].
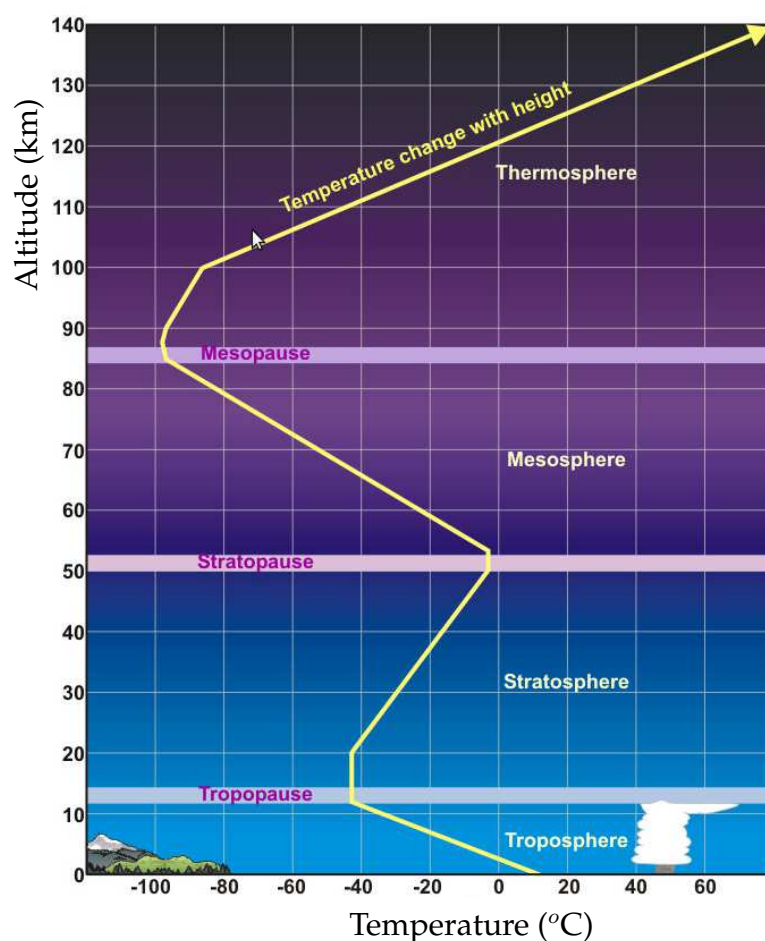
Figure 2.1: Standard temperature profile as a function of height. Source: University of Illinois website (http://www.atmos.illinois.edu/).

4

2.1.2 Absorption and emission

Solar radiation interacts with the air molecules. When a molecule absorbs or emits a photon, its energy changes. By absorption of a photon, the molecule is transfered from a lower energy state to the higher, in contrast to emission, when the molecule is transfered to a lower energy level. In both emission and absorption, the energy gap between the levels is equal to the energy of the absorbed/emitted photon. The probability of absorption or emission by a molecule depends on the wavelength of incoming radiation and the structure of the molecule. This probability is defined as an absorption cross section, σ_a. In other words, the absorption cross section is the cross-sectional area of a molecule which absorbs the incident radiation. The absorption cross section may change with temperature, wavelength and pressure.

Molecules, in general, absorb and emit energy at discrete wavelengths. Thus, absorption or emission of an isolated molecule gives an unique line spectrum consisting of very narrow absorption or emission lines, separated by gaps in which the molecule is transparent to the incident radiation. Absorption in the infrared region will change the vibrational energy state of a molecule, while absorption in the microwave or millimeter wavelengths range leads to transitions between rotational levels. Highly energetic orbital transitions occur in the UV and visible regions, where the photon energy is comparable to that of the molecular bond. Hence, absorption in the UV and visible regions, may involve the destruction of the molecule, namely photo-dissociation. Note that orbital transitions may also be accompanied by vibrational and rotational transitions [Brasseur et al., 1999].

2.1.3 Scattering

Air molecules and particles scatter the solar radiation. A particle or molecule absorbs the energy from an incoming photon and re-emits the energy in all directions. The amount of scattering depends on the particle or molecule size and the wavelength of the incident beam. The ratio of particle or molecule size to the wavelength of incident radiation determines the type of scattering. Accordingly, Rayleigh scattering occurs when the diameter of the scatterer (d) is much smaller than the wavelength of the incident radiation (λ) and Mie scattering occurs when the diameter is almost the same size or larger than the wavelength. UV-visible radiation is scattered by atmospheric molecules (Rayleigh), while scattering is negligible for the microwave range. Particles and cloud droplets contribute to Mie scattering.

The Rayleigh phase function for air molecules is given as $P(\psi) = \frac{3}{4}(1 + \cos^2 \psi_s)$, where ψ_s is the scattering angle, which is the angle between the incoming and the scattered radiation. Rayleigh scattering is isentropic and half of the radiation is scattered backwards and the other half in forward direction. The Mie phase function is more complicated and varies with the shape, size, concentration and chemical composition of the particle as well as the polarization of the incident radiation. Particles may also contribute to absorption besides scattering [Brasseur et al., 1999].

2.2   Stratosphere

The atmosphere is composed of nitrogen, oxygen, carbon dioxide, argon and minor trace gases. Nitrogen ($\sim$78%) and oxygen ($\sim$21%) are the most abundant constituents. However, the chemical composition of the atmosphere is changing all the time due to the interaction with the Earth's surface and human activities. The troposphere is homogeneous because of vertical mixing and turbulence. In the stratosphere the nitrogen molecules are stable but oxygen molecules are photolysed by short wavelength radiation. Among those species emitted in the troposphere, some species which have longer life-time can reach the stratosphere via transport through the tropical tropopause, where they may undergo chemical transformation by photolysis processes or reaction with radicals generated by photolysis of other species. Not only oxygen photolysis which leads to ozone formation governs the chemistry of the stratosphere, but also the catalytic reaction chains engaging odd oxygen (O_x) determine the composition of this layer. Changes of the stratospheric composition and circulation have a large impact on the whole atmosphere and in general on the Earth system. The combined effect of ozone reduction in the stratosphere and the enhancement of carbon dioxide and other green-house gases in the atmosphere cause cooling of the stratosphere.

Chemical species in the stratosphere are grouped as source gases, reservoirs and reactive species. Source gases are the long-lived species which can survive the transport from the tropical troposphere to the stratosphere (e.g., H_2O, CFCs, N_2O). When reaching the stratosphere, source gases undergo transformation by UV photo-dissociation or by reaction with the chemicals initiated by UV rays. In this process, source gases either produce short-lived reactive species like radicals (e.g., OH, NO_2, ClO, Br) or species which quickly can form radicals. Source gases may also generate reservoir species which have longer life-time and are much less reactive than radicals (e.g., HCl, HNO_3, $BrONO_2$). The reservoirs with high water solubility (e.g., acids like HCl, HNO_3, HF) are washed away from the atmosphere by precipitation. Figure 2.2 gives a schematic illustration of source, reactive and reservoir species in the stratosphere.

In the following sections the ozone chemistry in the stratosphere and ozone loss reaction chains will be discussed.

2.2.1   Ozone chemistry

Ozone molecules consist of three oxygen atoms. Ozone is one of the most important constituents of the stratosphere sustaining life on Earth by absorbing the damaging UV radiation. The ozone layer lies between 20 to 40 km, while its peak in volume mixing ratio (8-11 ppmv) is located around 35 km. The number density peak of ozone is however situated at a lower altitude of about 15–25 km, since pressure decreases exponentially with increasing height. Figure 2.3 shows the ozone profile in number density and volume mixing ratio units for the equator, mid-latitudes and the Arctic (0°, 40 ^{o}N
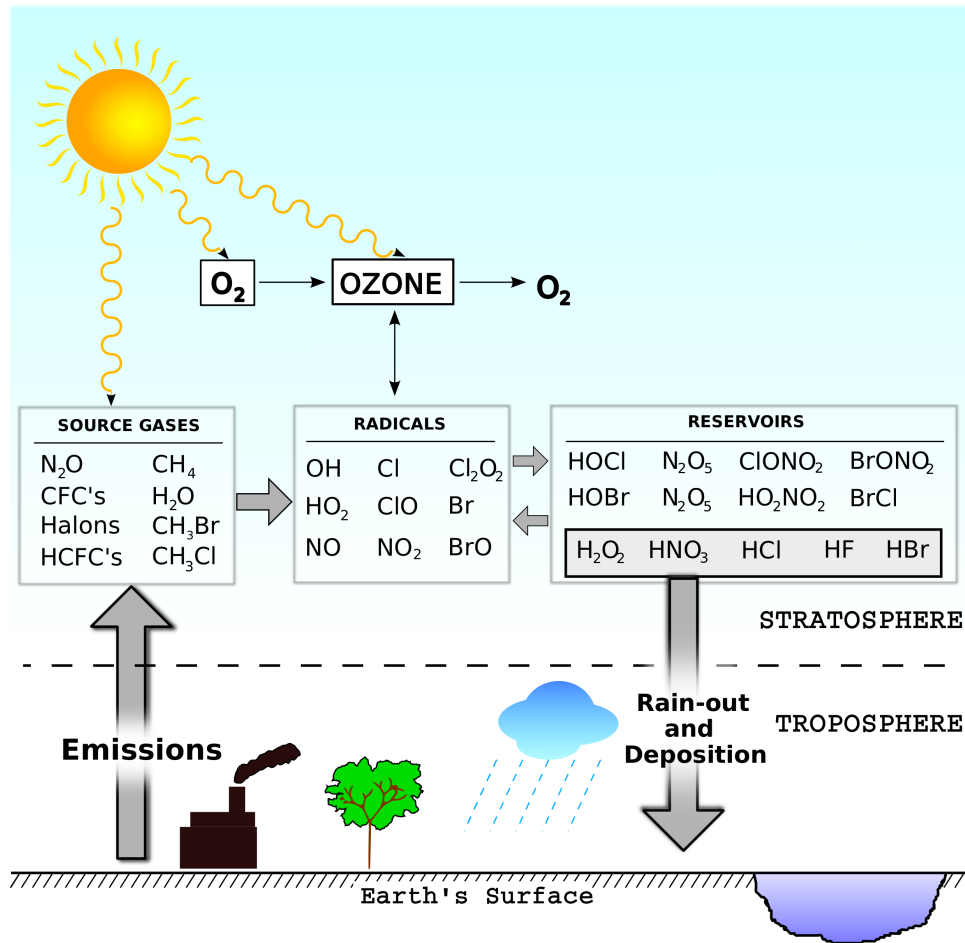
Figure 2.2: Schematic diagram of the source, reservoir and reactive species in the stratosphere. Inspired from Brasseur et al. [1999].

and 80°N) between 10 to 60 km. The absorption of UV light by ozone molecules leads to the negative lapse rate and increasing temperature in the stratosphere. The Dobson Unit, DU, is a measure of total column ozone as the number density integrated from surface to the top of atmosphere. One DU is equivalent to the thickness of a 0.01 mm ozone column when brought to standard temperature and pressure (273 K and 1 atm). Typically, the total ozone column at mid-latitudes varies between winter and summer in the range of 300-400 DU. Ozone is mostly produced in the tropical stratosphere, where the solar flux is maximum, and is transported polewards by the stratospheric circulation (Brewer-Dobson), where it accumulates. Ozone formation and destruction in the stratosphere is described by the Chapman reactions formulated in the late 1920s:

$$O_2 + h\nu(\lambda < 242\text{nm}) \longrightarrow 2O \tag{2.4}$$

$$O + O_2 + M \longrightarrow O_3 + M \tag{2.5}$$

$$O_3 + h\nu(\lambda < 336\text{nm}) \longrightarrow O(^1D) + O_2 \tag{2.6}$$

$$O + O_3 + M \longrightarrow 2O_2 + M \tag{2.7}$$
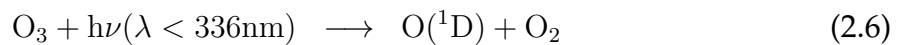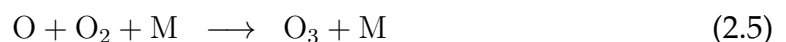
Here hν is the energy of a photon and M symbolizes any molecule (third body)
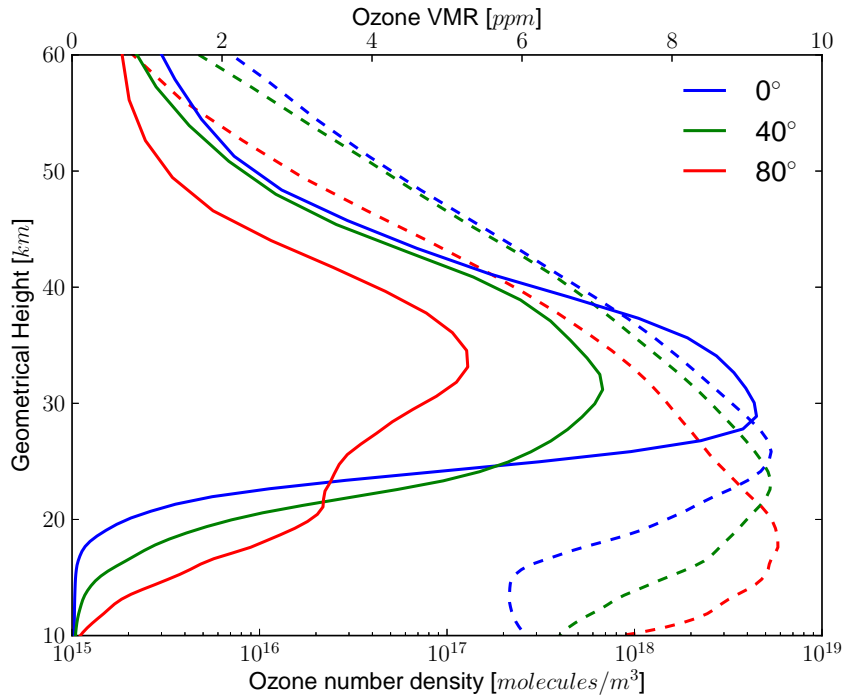
Figure 2.3: Ozone profiles from ECMWF for 2009-12-01, plotted for the tropics (0°), mid-latitudes (40°N), and high-latitude (80°N) regions. Solid and dashed lines correspond to volume mixing ratio [ppmv] and number density [molecules/m^3], respectively.

which removes the excess energy after collision. O(^1D) denotes the atomic oxygen in an excited state. The excess energy acquired by M in reaction 2.5 is in the form of thermal energy and heats up the stratosphere. Reaction 2.5 is more significant in the upper stratosphere or at low latitudes, where the concentration of O is high. As these reactions show, both O$_2$ and O$_3$ absorb radiation below 242 nm. The two first reactions produce ozone, while the two latter deplete ozone. Since atomic oxygen and ozone interconvert quickly, the sum of O, O$_3$ and O(^1D) is defined as odd oxygen, O$_x$. Reactions 2.5 and 2.6 are fast and cycle O$_3$ and O back and forth. As altitude increases, reaction 2.5 becomes slower and reaction 2.6 becomes faster, which makes the atomic oxygen the dominant form of odd oxygen at high altitudes and ozone, the dominant constituent of odd oxygen below almost 60 km [Wayne, 2000]. Although formation of ozone depends on photolysis reactions, stratospheric ozone shows only a weak diurnal variation. Below 40 km, the source reactions 2.4 and 2.6 are switched off after sunset, but the remaining O atoms will continue to generate ozone molecules via reaction 2.5. This means that the ozone formation continues during the darkness. At altitudes above 45–50 km the day-night concentrations change more significantly due to the faster O$_3$ photolysis and slower formation rate (reaction 2.5) [Wayne, 2000].

The global distribution of ozone is not only determined by photochemistry, but also affected by transport in the middle atmosphere. O(^1D) is produced exclusively by photochemistry (reaction 2.6), so its concentration depends on the local photochemical conditions [Brasseur and Solomon, 2005]. The life-time of O(^1D) is rather short com-

pared to a typical time scale for meridional transport. O_x has a longer life-time to be influenced by transport processes and can represent the total ozone. The maximum peak of the ozone profile does not correspond with the altitude of the highest oxygen photolysis rate. Larger ozone densities are found at polar latitudes and lower altitudes, however most of ozone is formed at the equator and higher altitudes. This can be explained as the ozone-rich air from the equator cools and therefore becomes heavier and sinks to lower altitudes as it moves poleward [Wallace and Hobbs, 2006, Wayne, 2000]. Figure 2.3 shows the maximum of ozone in the polar stratosphere below 20 km (in terms of number density), while at mid-latitudes and in the tropics it is located at higher altitudes.

The observed concentrations of ozone, especially in the mid-latitude and polar stratosphere, could not be explained by the Chapman reactions only. Reactions 2.6 and 2.7 are not the sole reactions depleting ozone, as radical species generated in the stratosphere can, even more efficiently, destroy ozone. The catalytic cycle which removes odd oxygen from the stratosphere can be written as:

$$X + O_3 \longrightarrow O_2 + XO \tag{2.8}$$

$$O + XO \longrightarrow O_2 + X \tag{2.9}$$

$$\text{Net}: O + O_3 \longrightarrow 2O_2 \tag{2.10}$$

X represents a catalyst (Br, Cl, NO and OH) and XO is an intermediate product. These reactions are usually faster than the Chapman reactions. The main characteristic of catalytic reactions is that X is consumed in reaction (2.8), but is regenerated in the reaction (2.9), so just a few molecules can deplete a large amount of ozone. The reaction cycle represented by 2.8 and 2.9 is important in the middle and upper stratosphere, because oxygen atoms are more abundant at higher altitudes (Garcia and Solomon [1994]).

2.2.2 HO_x chemistry

Odd hydrogen, HO_x, comprises the sum of H, OH and HO_2. The HO_x cycle is the first catalytic cycle recognized to be involved in ozone destruction and is initiated by OH radicals. The HO_x cycle dominates ozone destruction in the lower stratosphere (below 20 km) as well in the upper stratosphere and mesosphere (above 45 km). In the upper stratosphere and mesosphere, where the atomic oxygen is more abundant, OH can be formed from water and methane molecules, which ascend from the tropical troposphere into the stratosphere and mesosphere. Water in reaction 2.11 is the largest source of HO_x in the stratosphere, because it is more abundant than methane and hydrogen.

$$H_2O + O \longrightarrow 2OH \tag{2.11}$$

$$CH_4 + O \longrightarrow CH_3 + OH \tag{2.12}$$

$$H_2 + O \longrightarrow OH + H \tag{2.13}$$

The HO_x cycle destroys ozone at altitudes below $30\,km$ via the following reactions:

$$OH + O_3 \longrightarrow HO_2 + O_2 \tag{2.14}$$
$$HO_2 + O_3 \longrightarrow OH + 2O_2 \tag{2.15}$$
$$Net:\ 2O_3 \longrightarrow 3O_2 \tag{2.16}$$
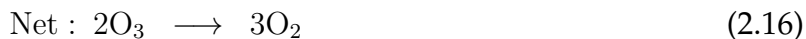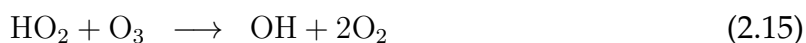
In the middle stratosphere below $40\,km$, where atomic oxygen is more abundant, another HO_x cycle destroys odd oxygen:

$$OH + O_3 \longrightarrow HO_2 + O_2 \tag{2.17}$$
$$HO_2 + O \longrightarrow OH + O_2 \tag{2.18}$$
$$Net:\ O + O_3 \longrightarrow 2O_2 \tag{2.19}$$
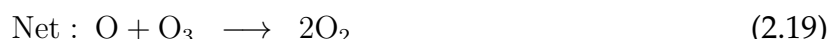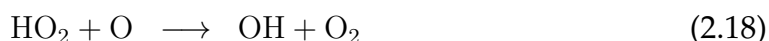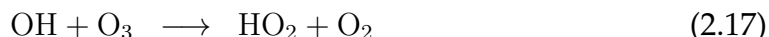
Above $40\,km$ the two cycles below become more important:

$$OH + O \longrightarrow H + O_2 \tag{2.20}$$
$$H + O_2 + M \longrightarrow HO_2 + M \tag{2.21}$$
$$HO_2 + O \longrightarrow OH + O_2 \tag{2.22}$$
$$Net:\ 2O \longrightarrow O_2 \tag{2.23}$$

and

$$OH + O \longrightarrow H + O_2 \tag{2.24}$$
$$H + O_3 \longrightarrow OH + O_2 \tag{2.25}$$
$$Net:\ O + O_3 \longrightarrow 2O_2 \tag{2.26}$$
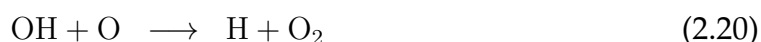
The partitioning of odd hydrogen determines which set of reactions leads to destruction of odd oxygen at different altitudes. The loss of HO_x is through recombination of OH and HO_2 which forms water vapor [Wallace and Hobbs, 2006, Brasseur et al., 1999]. The HO_x family is involved in reactions with species of the nitrogen, bromine and chlorine families which also may lead to ozone loss. The catalytic cycles involving HO_x and chlorine monoxide, ClO, will be discussed in section 2.2.4 (reaction 2.37 to 2.40).
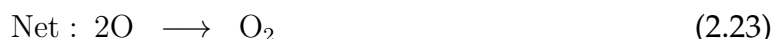
2.2.3 NO_x chemistry

Odd nitrogen (NO_x) comprises the sum of nitrogen oxides ($NO+NO_2+NO_3$) which are closely tied to each other via oxidation and photolysis reactions. The source of odd nitrogen species and related nitrogen compounds in the stratosphere is mostly the reaction of nitrous oxide (N_2O) with excited oxygen atoms, $O(^1D)$. Long-lived N_2O has both natural (mostly soil bacterial activities) and anthropogenic sources in the troposphere and is transported to the stratosphere, where it is destroyed by photolysis and reaction with $O(^1D)$. NO and NO_2 interconvert quickly and in this conversion they consume odd oxygen. The catalytic cycle involving the nitrogen family was suggested in 1970 as ozone destruction cycle. The ratio of odd nitrogen to total nitrogen

compounds (NO_x/NO_y) is an indicator of the ability of odd nitrogen to destroy strato-spheric ozone. NO initiates two catalytic cycles. The first cycle involves both ozone and atomic oxygen and is thus dominant in the middle stratosphere where the concentration of both O and O_3 is high enough [Brasseur and Solomon, 2005]:

$$NO + O_3 \longrightarrow NO_2 + O_2 \tag{2.27}$$
$$NO_2 + O \longrightarrow NO + O_2 \tag{2.28}$$
$$\text{Net}: O + O_3 \longrightarrow 2O_2 \tag{2.29}$$
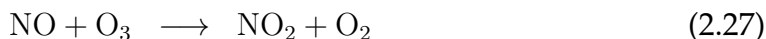
The other cycle, which does not require atomic oxygen, is more effective below 30 km:

$$NO + O_3 \longrightarrow NO_2 + O_2 \tag{2.30}$$
$$NO_2 + O_3 \longrightarrow NO_3 + O_2 \tag{2.31}$$
$$NO_3 + h\nu \longrightarrow NO + O_2 \tag{2.32}$$
$$\text{Net}: 2O_3 \longrightarrow 3O_2 \tag{2.33}$$

Nitrogen trioxide, NO_3, is mostly abundant at nighttime and is photolysed rapidly during the day. Odd nitrogen species have other catalytic destruction cycles which have minor importance for ozone loss and are not mentioned here. Examples are reactions of odd nitrogen molecules with the species of the chlorine family [Brasseur et al., 1999, Brasseur and Solomon, 2005].

2.2.4 Cl_x chemistry

Emission of long-lived Chloroflourocarbons (CFCs), which are the main anthropogenic contribution to the total chlorine budget of the atmosphere ($\sim$61%), are decreasing during the last decade. The main source of chlorine in the stratosphere is the transport of organic chlorine species (e.g. CFCs, HCFCs and CCl_4) from the troposphere followed by photo-chemical dissociation. Consequently, the negative trend of organic chlorine species has also decreased the stratospheric chlorine budget. The amount of chlorine is also controlled by air movements and mixing processes in the stratosphere. The time scale for the transport of species from the tropopause to the higher latitudes in the mid-latitude and polar stratosphere is about 3–6 years [WMO, 2010]. As the result, there is a time lag between the change of tropospheric and stratospheric concentrations. The evolution of the global total chlorine abundance (Cl_y) in the stratosphere (Figure 2.4) shows an increasing trend since 1975 until the late 1990s and a decreasing trend afterwards. The figure also shows the lag between the tropospheric and stratospheric abundances. A decreasing trend for the main inorganic chlorine reservoirs (HCl and $ClONO_2$) and the main reactive chlorine species (ClO) is also indicated by various observations [Rinsland et al., 2003, Solomon et al., 2006, Jones et al., 2011](see Figure 2.5). HCl and $ClONO_2$ are not directly involved in the chemical reactions depleting ozone, but the amount of active chlorine (ClO+ClOOCl+Cl) is proportional to the sum of the so called reservoir gases HCl and $ClONO_2$.
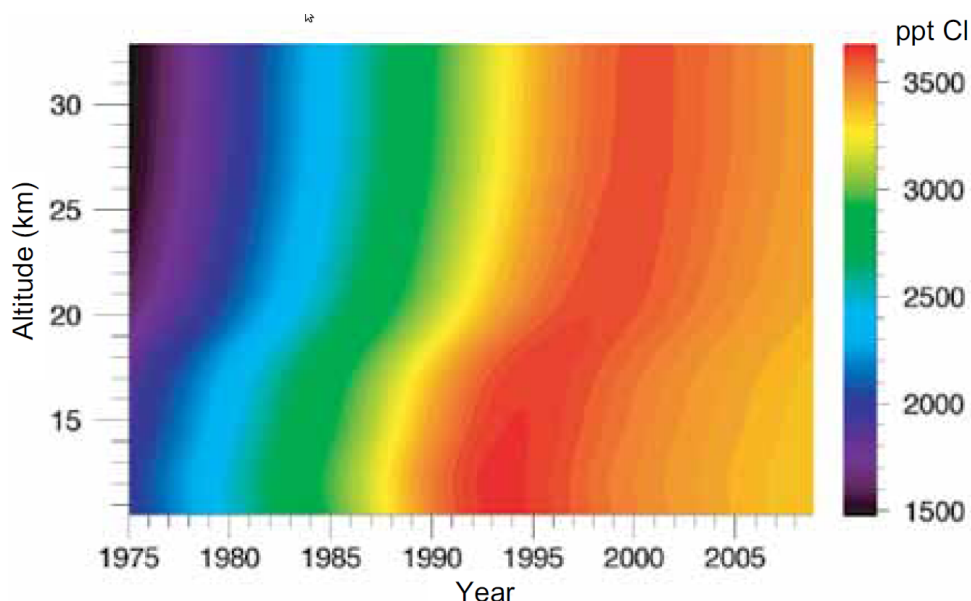
Figure 2.4: The evolution of total chlorine abundances in the stratosphere, calculated based on the global tropospheric chlorine measurement time series. Typical profiles of mean age of air in the stratosphere (derived from observations of SF_6 and CO_2) and a parametrization of the age spectrum are used for the calculation of the effects of mixing and transport in the stratosphere. Source: WMO [2010].

When organic chlorine species such as CFCs are photolysed in the stratosphere, Cl atoms are formed. The reactions between the free Cl atoms and ozone molecules leads to formation of chlorine monoxide radicals, ClO, which is the main constituent of active chlorine. Cl and ClO are both active species which have the ability to destroy ozone:

$$Cl + O_3 \longrightarrow ClO + O_2 \qquad (2.34)$$
$$ClO + O \longrightarrow Cl + O_2 \qquad (2.35)$$
$$Net : O + O_3 \longrightarrow 2O_2 \qquad (2.36)$$

The above cycle is more important in the upper stratosphere. This cycle continues until Cl and ClO are converted to the reservoir species, HCl and $ClONO_2$ by reaction with NO_2 and CH_4. HCl has the longest life-time and is the most abundant inorganic stratospheric chlorine species. It constitutes more than 95% of the chlorine species above 50 km [WMO, 2010]. $ClONO_2$ is an important reservoir at altitudes below 30 km where it is rapidly formed. In fact, $ClONO_2$'s ability to act as the reservoir is limited by photolysis or reaction with O atoms, leading to formation of Cl atoms. Hypochlorous acid, HOCl, is another chlorine reservoir which is not as abundant as HCl and $ClONO_2$ and is formed by reactions of species of the chlorine and odd hydrogen families.
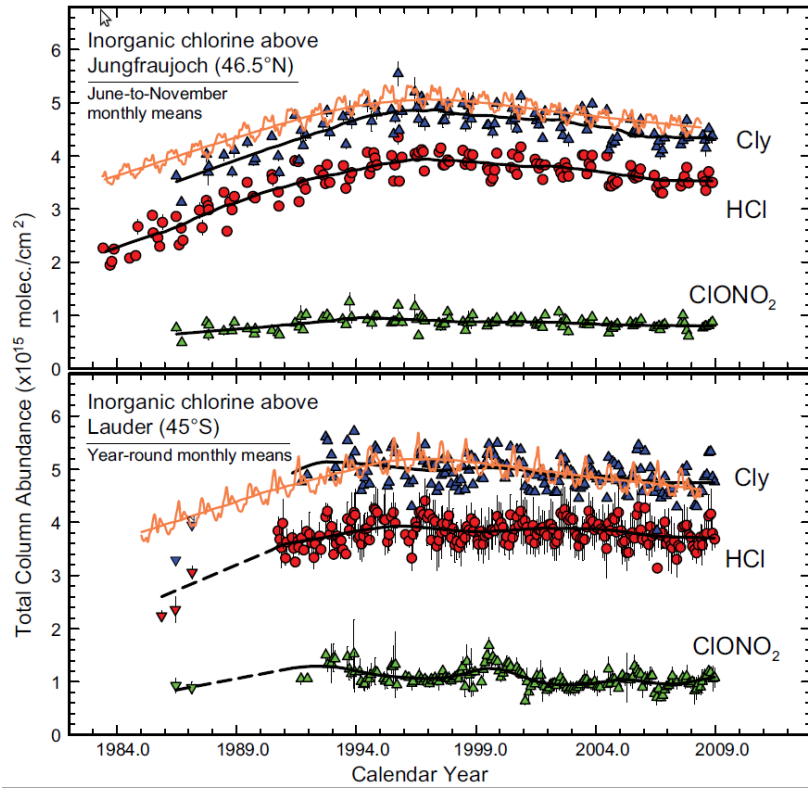
Figure 2.5: Time series of monthly mean total column HCl (red circles) and ClONO$_2$ (green triangles) abundance (molecules per square centimeter), as measured above the Jungfraujoch (46.5^{o}N) and Lauder (45°S). Cl$_y$ column estimates (blue triangles) are the sum of HCl and ClONO$_2$ columns. Jungfraujoch data are shown only for June to November of each year; results from all months are displayed for Lauder. Fits to the datasets are given by the black curves. The orange curves and corresponding fits represent Cl$_y$ (HCl+ClONO$_2$) from the University of Leeds 2-D model. Source: WMO [2010].

$$
\begin{aligned}
\text{Cl} + \text{O}_3 &\rightarrow \text{ClO} + \text{O}_2 & (2.37) \\
\text{OH} + \text{O}_3 &\rightarrow \text{HO}_2 + \text{O}_2 & (2.38) \\
\text{ClO} + \text{HO}_2 &\rightarrow \text{HOCl} + \text{O}_2 & (2.39) \\
\text{HOCl} + \text{h}\nu &\rightarrow \text{OH} + \text{Cl} & (2.40) \\
\text{Net}: 2\text{O}_3 &\rightarrow 3\text{O}_2 & (2.41)
\end{aligned}
$$

The latter cycle is more important at lower altitudes (below 20 km) [Brasseur et al., 1999]. It accounts for about 30% of the ozone loss due to halogens in the mid-latitude lower stratosphere [Wennberg et al., 1994]. There are another ozone destruction cycles involving reactions of species of the chlorine and odd nitrogen families. In such cycles, the ozone loss can not be attributed to just the chlorine family as species from different families are involved.

2.2.5 Br_x chemistry

Although bromine species are less abundant in the atmosphere, they are more effective than chlorine at destroying stratospheric ozone. It is partly due to the larger absorption cross sections of bromine species compared to chlorine compounds which leads to a faster photolysis rate for bromine species, resulting to faster conversion of bromine compounds to active forms (Br and BrO). There are no stable bromine reservoirs for active bromine species like chlorine species, because HBr and $BrONO_2$ are short-lived and less abundant and have less formation channels than HCl and $ClONO_2$. The main source of bromine in the stratosphere is photo-dissociation of organic bromine species from natural and anthropogenic sources (e.g., CH_3Br and halons), which release Br atoms. Reactions of Br with ozone molecules form bromine monoxide. The bromine catalytic cycle including reactions 2.8 and 2.9 takes place in the stratosphere. When bromine containing species reach the stratosphere via the tropical tropopause the species are photolysed and release bromine atoms. The total stratospheric bromine budget is estimated to be about 21 ± 5 pptv [McLinden et al., 2010]. BrO_x, active bromine, is the sum of BrO and Br. The reactions coupling BrO and ClO enhances the bromine effectiveness in ozone destroying cycles.

$$BrO + ClO \rightarrow Br + Cl + O_2 \tag{2.42}$$
$$Br + O_3 \rightarrow BrO + O_2 \tag{2.43}$$
$$Cl + O_3 \rightarrow ClO + O_2 \tag{2.44}$$
$$Net: \qquad 2O_3 \rightarrow 3O_2 \tag{2.45}$$
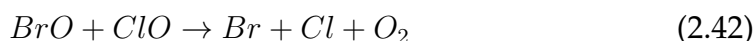
The catalytic cycle involving BrO and HOBr similar to the chlorine analogue (reactions 2.37 to 2.40), accounts for about 20–30% of the ozone loss associated with halogens in the mid-latitude lower stratosphere [Wennberg et al., 1994]. Reactive bromine species in the stratosphere are short-lived. During the day and below about 40 km, BrO is the most abundant form of active bromine (BrO_x). HOBr is the second most abundant during daytime at the same altitude. During nighttime and below 40 km, $BrONO_2$ is the dominant form of active bromine [Brasseur et al., 1999, Brasseur and Solomon, 2005].

2.3 Chemical reactions

The rate of a reaction is defined as the temporal change of the concentration of a species. The reaction rate describes how fast a reaction occurs. The chemical reactions in the atmosphere break down in three categories, namely unimolecular, bimolecular and termolecular reactions. The concentrations of chemical species depend on the rate they are produced or destroyed. A general form of chemical reactions and the reaction rate can be written as:

$$aA + bB + cC + ... \rightarrow mM + nN + ... \tag{2.46}$$

$$Rate = -\frac{1}{a}\frac{d[A]}{dt} = -\frac{1}{b}\frac{d[B]}{dt} = -\frac{1}{c}\frac{d[C]}{dt} = +\frac{1}{m}\frac{d[M]}{dt} = +\frac{1}{n}\frac{d[N]}{dt} \tag{2.47}$$

The reaction rate (molecule $cm^{-3}s^{-1}$) is related to the rate of change of a reactant or of a product and can be expresses as:

$$Rate = -k[A]^a[B]^b[C]^c...$$ (2.48)

Where k is the reaction rate constant (coefficient) and [A], [B] and [C] are the concentrations of the reactants. The exponents (a, b, c,...) are reaction orders which depend on the reaction mechanism. In many cases, the reaction rate coefficients change with temperature and pressure. This section attempts to give a general description of the gas-phase atmospheric reactions and their rate coefficients in the atmosphere. These sections (section 2.3 to 2.3.4) are based on the books and descriptions of Brasseur et al. [1999], Wayne [2000] and Sander et al. [2009, 2011]. The parameters required for the calculation of reaction rate constants are tabulated in JPL publications on kinetics of reactions in the stratosphere for the most important atmospheric reactions.

2.3.1 Unimolecular reactions

Unimolecular or first order reactions involve one reactant. The decomposition of a particle is an example of such reactions and can be expressed as

$$A(+M) \rightarrow products.$$ (2.49)

M could be any molecule (most probably O_2 or N_2) which carries away excess energy. The rate of this reaction is given as

$$Rate = -\frac{d[A]}{dt} = k_u[A],$$ (2.50)

where k_u is the reaction rate constant [time^{-1} or s^{-1}] and A is the reactant concentration. These reactions are strongly temperature and pressure dependent. The collisions increase at higher temperatures and pressures, so these reactions are faster in such conditions. In addition, some species are thermally unstable and decompose at higher temperatures.

2.3.2 Bimolecular reactions

Bi-molecular reactions are the most common reactions in the atmosphere. These reactions involve the collision between two reactants and are also called two body or second order reactions.

$$A + B \rightarrow products$$ (2.51)

The rate at which the reactions proceeds is:

$$Rate = -\frac{d[A]}{dt} = -\frac{d[B]}{dt} = k_b[A][B],$$ (2.52)

where k_b is the reaction rate constant in [cm^{3}molecule^{-1}s^{-1}] and A and B are the reactant concentrations. The temperature dependence of the rate constants of many bimolecular reactions are expressed by the Arrhenius equation:

$$Rate = A_r e^{-\frac{E_a}{RT}}. \tag{2.53}$$

R is the universal gas constant and T is the temperature (in Kelvin). A_r is the pre-exponential factor and E_a is the activation energy. The value for A_r, E_a are tabulated in the JPL publications on kinetics of reactions in the stratosphere [Sander et al., 2011].

2.3.3 Termolecular reactions

Termolecular reactions involve three molecules, however the reaction does not occur by a single collision. A and B are the reactants and M is the third body or collision partner and in most cases represent O$_2$ and N$_2$, which assists the reaction by taking away the excess energy.

$$A + B + M \rightarrow products \tag{2.54}$$

The rate at which the reaction proceeds is:

$$Rate = -\frac{d[A]}{dt} = -\frac{d[B]}{dt} = -\frac{d[C]}{dt} = k_t[A][B][C]. \tag{2.55}$$

Here, the rate constant for the termolecular reactions are expressed as, k_t, in [cm^{6}molecule^{-2}s^{-1}] units. k_t is parametrized as:

$$k_t = \frac{k_\infty k_0[M]}{k_0[M] + k_\infty} F^{\left\{\left(1+[\log_{10}(\frac{k_0[M]}{k_\infty})]^2\right)\right\}^{-1}} \tag{2.56}$$

where k_0 and k_∞ can be expressed as a function of temperature by equation 2.57 and 2.58.

$$k_0(T) = k_0(300K)\left(\frac{T}{300}\right)^{-n} \tag{2.57}$$

$$k_\infty(T) = k_\infty(300K)\left(\frac{T}{300}\right)^{-m} \tag{2.58}$$

Here, k_0 and k_∞ at 300 K as well as n and m should be known to be able to calculate the rate constant. These parameters can be determined experimentally by fitting the experimental values of K and assuming F as 0.6. A value of F set to 0.6 can best represent the pressure dependence of many atmospheric reactions [Brasseur et al., 1999]. These parameters are tabulated in JPL publications on kinetics of reactions in the stratosphere for termolecular reactions [Sander et al., 2011].

2.3.4   Photolysis (photo-dissociation) reactions

The photolysis reactions are unimolecular reactions in which the molecule is usually splitted into two radical fractions. These radicals are very reactive and short-lived (their life-time could be a fraction of a second) and may quickly react with other molecules.

$$A + h\nu \rightarrow B + C \tag{2.59}$$

B and C are the products of the reaction and $h\nu$ denotes the photon energy. The rate of reaction 2.59 is defined as:

$$Rate = -\frac{d[A]}{dt} = J[A] \tag{2.60}$$

J represents the photolysis rate (photolysis frequency) in unit of s^{-1}. The photolysis rate is a function of light intensity and molecule properties (e.g. absorption cross section and quantum yield). The photolysis rate is defined by the wavelength integrated product of the incoming solar irradiation (also called solar flux) and the absorption cross section of the absorbing molecule and the quantum yield (quantum efficiency). The photolysis rate of a reaction can be calculated as:

$$J = \int_{\lambda} \phi(\lambda)\sigma_a(\lambda)F(\lambda)d\lambda \tag{2.61}$$

σ_a is the absorption cross section of the molecule and $F(\lambda)$ is the spherically integrated actinic flux. The quantum yield, ϕ, represents the fraction of molecules which undergo photochemistry following photon absorption. By another word, the quantum yield is the efficiency of a photochemical process in absorbing photons and therefore is given by the ratio of number of excited molecules to the total number of photons absorbed. Absorption cross section and quantum yield are basic properties of the molecule and can be determined by laboratory experiments. Absorption cross sections and quantum yield may vary with temperature and pressure. The solar flux also varies with altitude, atmospheric composition and solar zenith angle. As a result, photolysis rates also vary with temperature, pressure, altitude and the solar zenith angle of the incident radiation [Brasseur et al., 1999].

2.4   Life-time of species

The chemical life-time of species can be defined as the time a molecule resides in the atmosphere before it is removed by some processes. It is a measure of how fast the concentration of a species would change. The shorter the life-time of a species, the faster its concentration reaches an equilibrium state with other molecules. The life-time of a molecule, τ, depends on the reactivity of the molecule. The life-time of molecule A in a first-order reaction (unimolecular) is defined as the time needed that the concentration of A drops to a fraction $\frac{1}{e}$ of its initial concentration and is given by the reciprocal of the first-order reaction rate constant $\frac{1}{k_u}$;

$$\tau_A = \frac{1}{k_u} \tag{2.62}$$
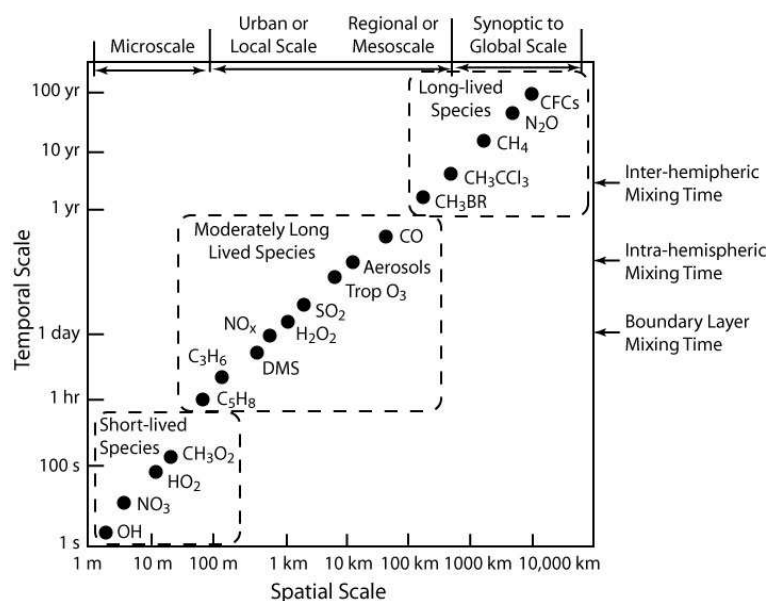
Figure 2.6: Temporal and spatial variability of some tropospheric constituents. Source:www.oceanworld.tamu.edu .

The life-time of a molecule in second-order (bimolecular) and third-order (termolecular) reactions also depends on the concentrations of the other reactants. This approximation is only valid if the concentration of the other reactant is constant within the time scale of τ_A. Equations 2.63 and 2.64 express the life-time of molecule A in bimolecular and termolecular reactions, respectively:

$$\tau_A = \frac{1}{k_b[B]} \tag{2.63}$$

$$\tau_A = \frac{1}{k_t[B][C]} \tag{2.64}$$

Here $[B]$ and $[C]$ denote the concentration of the other reactants and k_b and k_t are the reaction rate constants of bimolecular and termolecular reactions, respectively. The life-times of chemical species in the atmosphere are of the order of seconds (short-lived) to years (long-lived). Figure 2.6 shows the spatial and temporal variability of molecules depending on their life-time in the troposphere. Long-lived species are well mixed in the atmosphere, and their concentrations are influenced by atmospheric dynamics (e.g. N_2O, CH_4, CFCs). Short-lived species (e.g. radicals) have more variable concentrations depending on local processes such as photochemistry and are not directly influenced by dynamics, except through the transport of their source and sink molecules [Brasseur et al., 1999].

The life-time of a species thus does not only depend on the chemical process in which the species is involved, but also the transport and mixing mechanisms play important roles. In the troposphere, vertical mixing is of the time scale of hours to days, while in the stratosphere the vertical mixing takes months to years. The life-time of photochemically active species (e.g. ozone) depends on the altitude, for example the

ozone life-time at the equator can vary from 3 years at about 15 km to 2 days at an altitude of 40 km. At higher altitudes, ozone is mostly produced locally, but at lower altitudes it has a longer life-time and can be transported from the equator to the poles [Wayne, 2000].

2.5   Atmospheric models

An atmospheric model is a set of mathematical equations and algorithms which attempts to replicate the chemical and physical processes occurring in the atmosphere. The atmospheric models are implemented as computer codes and solve numerical equations. In general, models are our tools to test hypotheses that need to be verified by observations. The use of atmospheric models and the validation with measurements provides a tool to identify deficits in the current knowledge of atmospheric mechanisms. The models can also provide information about the future of the atmospheric state and weather and climate forecasts. In particular, chemistry models simulate the spatial distribution and temporal evolution of the chemical species in the atmosphere and their interaction with each other. Chemistry models are used to interpret field observations or experiments and to verify key variables. They can also be used to test the sensitivity of variables to complex chemical and physical processes.

The degree of detail and complexities in the Earth's atmosphere models is restricted to the initial purpose and computing power limitations. The hierarchy of atmospheric models includes, zero-, one-, two-, and three dimensional models and will be described in the following sections. The content of these sections are taken from Brasseur et al. [1999], Jonsson [2006], Wayne [2000].

2.5.1   Zero dimensional models or box models

Box models are the simplest models which focus on local processes. They solve the evolution of physical or chemical properties in time for a single point. With this type of model, even relatively complicated processes can be studied with a reasonable amount of computation. Chemical box models assume that the chemical reactions occur in isolated boxes. The air mass in the boxes is parametrized with simple concepts. The best use of the box models is to study the photochemistry in regions of the atmosphere where transport is negligible and production and loss rates of species dominate. Thus, one of the applications of box models is the investigation of the kinetics of chemical reactions or the influence of specific reactions. For this purpose, the model is fixed to one location as the reactions or the kinetic parameter is varied between different model runs.

2.5.2   1-dimensional models

One-dimensional models are the first extension of box models and the second step in the model hierarchy. If several box models are piled up on top of each other, a simple 1-d model is achieved without any transport between the boxes. One-dimensional models can be designed to take the vertical transport into account, however transport through large-scale circulations can not be represented. The vertical transport is represented by eddy diffusion, which is determined empirically. One-dimensional models are used to simulate the vertical distribution of atmospheric species without any latitudinal and longitudinal variation. One of the applications is to compare the 1-D model with the observations of vertical profile or diurnal variation of stratospheric and mesospheric species against local time or solar zenith angle (my first and second paper). If the model uses small time intervals, neglecting the horizontal transport does not affect the results significantly. In a chemical 1-D model, each chemical species is handled individually. The time evolution of the concentrations for each species is represented by a differential equation. A system of differential equation which is typically nonlinear and numerically stiff is solved. Such models are suitable for the analysis of global budgets of long-lived species and of local budgets of short lived species.

2.5.3   2-dimensional models

Two-dimensional models calculate the atmospheric boxes in two directions, namely in the altitude and latitude directions. In these models, each three dimensional field is longitudinally averaged, also called zonal mean, assuming the variation in longitude direction is negligible compared to variation in vertical and latitudinal directions. The dynamical processes can be better simulated by 2-D models, particularly in the stratosphere and mesosphere where homogeneous conditions exist. Due to the smaller computational efforts, two-dimensional models are widely used to simulate 3-dimensional phenomena such as winds and waves. Accounting for transport, two-dimensional models enable studies like the assessment of ozone trends or prediction of future changes in ozone or other chemical species. One disadvantage of 2-D models is that some processes such as heterogeneous chemistry and the variability of species near the tropopause are rather localized and should not be zonally averaged. Some attempts have been made to address this issue by parametrization which allows some zonal differences to be considered. The highly parametrized models, however, can be tuned to an arbitrary or sometimes unphysical manner.

2.5.4   3-dimensional models

Three dimensional models can more completely simulate the atmosphere, by considering the radiation, chemistry and dynamics of the atmosphere. By taking the vertical component of the wind fields instead of the eddy diffusion, these models enable a more realistic representation of vertical transport. They also reproduce waves and the meridional transport based on a more physical parametrization than 2-D models.

These models are used for weather predictions or future climate prediction. Global chemical transport models (CTM), general circulation models (GCM) and chemistry-coupled climate models (CCM) are some examples of 3-D models. Three dimensional models can include feedback mechanisms. In coupled 3-D models, the general circulation (the dynamics) is coupled and thus solved simultaneously with a chemistry model. This approach is computationally more expensive, but the fully coupled dynamics and chemistry is required for studies of stratospheric heating rate. Some attempts have been made to deal with the complexities of 3-D chemical models. For instance, in decoupled CTMs, the model is first run without chemistry, in order to calculate the dynamics and meteorological parameters such as winds and temperatures. These information are then are used as input variables for another 3-D chemical model, which then updates the chemistry by using advection. Consequently, the simulation of global or a specific region for shorter time periods can be done with less computational loads. Such simplification is valid as long as the chemistry does not alter the dynamics of the atmosphere. 3-D models can be simplified using meteorological analyses to get the temperature and wind fields. The disadvantage of such an approach is that there is no feedback between chemistry and meteorology. This approach may be sufficient in the troposphere, where the coupling between chemistry and dynamics is weaker [Wayne, 2000].

2.5.5 The structure of chemistry models

The continuity equation is the basic equation for the calculation of the concentrations in a chemical model. The continuity equation is based on mass conservation in an infinitesimal volume element. In terms of number density, n_i, the equation is expressed as:

$$\frac{\partial n_i}{\partial t} = P_i - L_i n_i - \nabla.(n_i v) \tag{2.65}$$

Here n_i is the number density of species i and P_i and L_i are the gross production and the loss coefficients. Note that, the loss rate for each species is proportional to its concentration. The last term, $\nabla.(n_i v)$, represents the transport and circulation, where v is the wind velocity vector.

The equation in one dimension (vertical) can be expressed as:

$$\frac{\partial n_i(z)}{\partial t} = P_i - L_i(z)n_i(z) - \frac{\partial}{\partial z}\left[K(z)N(z)\frac{\partial f_i(z)}{\partial z}\right] \tag{2.66}$$

The derivative respective to z represents vertical transport through mixing processes. f_i is the mixing ratio of species i and N is the number density of air. K is the diffusion coefficient which in one-dimensional models represents the molecular (eddy) diffusion.

Since the production and loss rates for any species depends on the concentration of other constituents, a system of equations should be solved for all interacting species.

In numerical models, the continuity equation is solved simultaneously for all chemical species regarding proper initial and boundary conditions. The differential equations for the kinetics are stiff, which means that the concentration of one species, may change rapidly as the concentration of another change slowly. By other words, the chemical life-time of the species vary by several order of magnitude. There are some methods to reduce the stiffness of the chemical schemes. The chemical species can be grouped into families, where they can be quickly inter-converted. Examples of such families are the odd oxygen (O_x), odd chlorine (ClO_x), odd nitrogen (NO_x) and odd hydrogen (HO_x) families.

2.6   The MISU-1D model

MISU-1D is a 1D photochemical box model incorporating detailed radiative transfer calculations in the UV and visible region and state of art stratospheric chemistry [Jonsson, 2006]. Multiple scattering and albedo effects are treated according to Lary and Pyle [1991]. The sphericity of the earth is taken into account which allows for non-zero transmitted flux at solar zenith angles greater than 90 degrees. The Earth-Sun distance is corrected for seasonal variations according to Madronich [1993]. The variability in the solar flux over the 11-year solar cycle is not considered in the model. The model includes a total of 120 reactions, constituting the most important gas-phase reactions in the stratosphere and mesosphere. The kinetic parameters for the calculation of rate constants and photolysis rates are mostly specified according to JPL 2009 recommendations, except for the reactions involving $HOCl$, HO_2 and HCl, which have been updated to JPL 2011 [Sander et al., 2011]. The input solar flux for the calculation of photolysis rates is adopted from the WMO [1986] reference spectrum. Ozone absorption cross sections and the oxygen absorption cross sections in the Schumann-Runge bands are in accordance with WMO [1986] recommendations and the Koppers and Murtagh [1996] algorithm, respectively. The Herzberg continuum is taken from Nicolet and Kennes [1986].

The model starts the simulations at 12:00 local solar time, when the solar zenith angle is minimum. The concentration of long-lived species is taken from measurements or output from other models (e.g. CMAM). The short-lived species are initialized with zero concentrations as they are formed quickly as the simulations start. The model then reads the cross sections for molecules involved in photolysis reactions and save them in an structure for further use in differential equations. If the cross sections are temperature or pressure dependent, they are re-calculated according to the temperature and pressure profiles. The reaction schemes are read from the databases and also saved to be used in differential equations. The calculation of photolysis rates for molecules involved in photolysis will be described in section 2.6.1. The differential equations are formed as the sum of all production and loss terms. The system of differential equations is stiff and is solved using the Shampine and Reichelt [1997] algorithm. Figure 2.7 illustrates the different parts of the MISU-1D model.
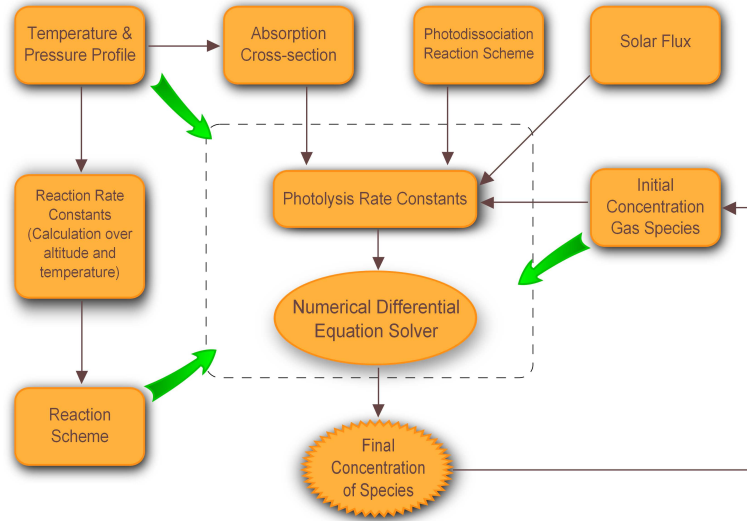
Figure 2.7: MISU-1D model structure, inspired from Jonsson [1996].

2.6.1   Radiation flux and photolysis rates in MISU-1D

The direct radiation flux in MISU-1D is treated assuming spherical geometry, while the scattered radiation is assumed plane-parallel. Pure absorption and scattering in the atmosphere is due to absorption of short-wavelength radiation ($\lambda <310\,\text{nm}$). Most of the short wavelength radiation is absorbed by oxygen and ozone molecules. The optical depth due to absorption in each layer of the model (dz) is calculated as

$$\tau_{abs} = \int_{z_1}^{z_2} (\sigma_{absO_2} N_{O_2} + \sigma_{absO_3} N_{O_3} + \sigma_{absN_2} N_{N_2}) l dz, \qquad (2.67)$$

where σ_{abs} and N represent the absorption cross sections and number densities for N$_2$, O$_2$ and O$_3$ molecules. l and z are path-length and altitude. The optical thickness caused by scattering is defined mostly by scattering of light by oxygen and nitrogen molecules which are the main constituents of the air.

$$\tau_s = \int_{z_1}^{z_2} (\sigma_{sO_2} N_{O_2} + \sigma_{sN_2} N_{N_2}) l dz \qquad (2.68)$$

Here σ_s denote scattering cross sections for oxygen and nitrogen molecules. The total optical thickness in each layer is the sum of τ_{abs} and τ_s.

The scattering field in the MISU-1D model is calculated according to Lary and Pyle [1991], which uses a plane-parallel approximation to calculate the source function at all heights and wavelengths for the solar flux incident at each solar zenith angle. In this method, photolysis rates are calculated using an enhancement factor defined as the total flux at any point (actinic flux $F(\lambda)$) normalized by the solar flux incident at the top of the atmosphere [Lary and Pyle, 1991]. The enhancement factor, $S(\lambda)$, varies with wavelength, solar zenith angle, altitude and surface albedo as well as ozone and temperature [Meier et al., 1982]. The total flux integrated over all wavelengths is used also for the calculation of photolysis rates at different altitudes in the model. The

following expression is used in the MISU-1D model for calculating the photolysis rates altered by multiple scattering.

$$J = \int_\lambda \phi(\lambda)\sigma_a(\lambda)F(\lambda)S(\lambda, z, X, A)d\lambda. \tag{2.69}$$

X is the solar zenith angle of radiation, z is the altitude and A represents the surface albedo. σ_a is the absorption cross section of a molecule, $F(\lambda)$ is the spherically integrated actinic flux and ϕ is the quantum yield.

Chapter 3

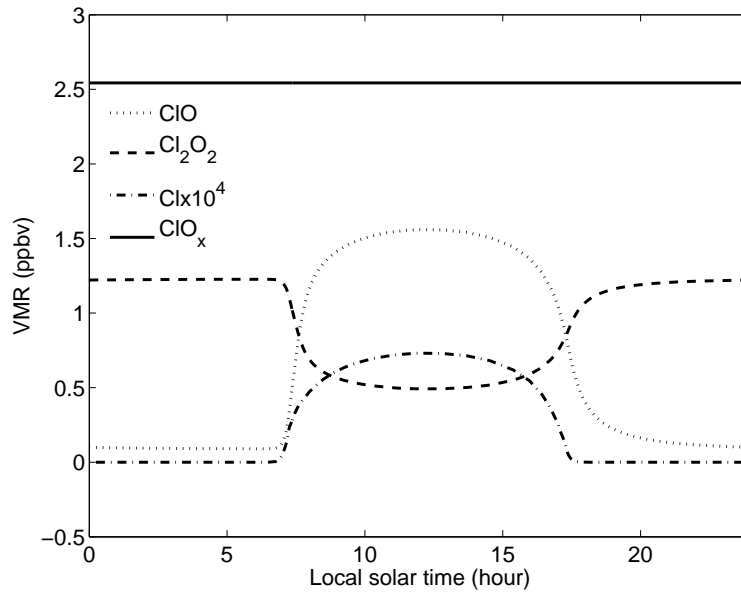# Study I: ClO diurnal variation in the Arctic lower stratosphere

This chapter describes the modeling of chlorine monoxide, ClO, and its diurnal variation in the winter Arctic lower stratosphere which is the subject of **paper I**. The results have been compared with observations made by the Airborne SUbmillimeter Radiometer (ASUR) during the winter of 1996, 1997 and 2000.

ClO is the key species in chlorine catalyzed ozone destruction cycles, globally and particularly in the polar lower stratosphere. ClO is the main constituent of reactive chlorine and is formed via heterogeneous reactions on polar stratospheric clouds. Consequently, studying of the temporal evolution of chlorine monoxide helps us to interpret the temporal ozone variations in the stratosphere. Elevated ClO concentrations in the Antarctic and Arctic stratosphere are coincident with low ozone concentrations. The first description of chlorine partitioning was given by Solomon and Garcia [1984].

Many reactions in the atmosphere are directly or indirectly influenced by solar radiation. That is the main reason of diurnal variation of species concentrations in the atmosphere. Formation of the ClO-dimer (ClOOCl or Cl_2O_2) is the result of the self reaction of ClO during nighttime. Figure 3.1 shows the partitioning between ClO and its dimer during the course of a day typical for the polar lower stratosphere. ClO increases sharply after sunrise and reaches its maximum value during daytime, due to the photo-dissociation of the ClO-dimer leading to the formation of Cl atoms. ClO is then formed by the reaction of chlorine atoms with ozone molecules during the day. These reactions and mechanisms are described in section 3.1.

3.1   ClO-dimer cycle

Halogen catalyzed ozone loss (particularly chlorine derived from CFCs or along with bromine) has been shown to be consistent with anti-correlation between elevated ClO and depleted ozone in the lower stratosphere inside the polar vortex during late-winter to early-spring. The heterogeneous reactions on stratospheric clouds convert chlorine
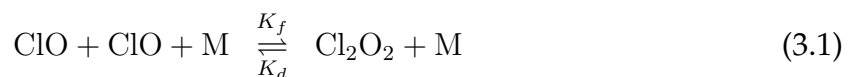
Figure 3.1: Diurnal variation of ClO, Cl_2O_2, Cl and assumed ClO_x ($[ClO]+2[Cl_2O_2]+[Cl]$) in the Arctic lower stratosphere (20 km) at a latitude of 70^oN during spring. The plot shows the volume mixing ratio of these species versus local solar time. Cl values have been magnified 10^4 times for better visualization.
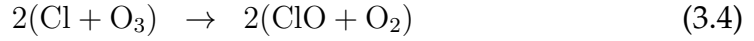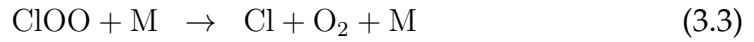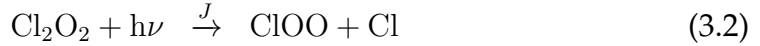
species from their reservoir forms (HCl and $ClONO_2$) into their active forms (Cl, ClO, ClOOCl). As the stratospheric clouds sink, they remove nitrogen (denitrification) and water (dehydration) from the stratosphere. Therefore the deactivation is delayed and chlorine may remain in its reactive form until late spring. Stratospheric clouds are formed at temperatures below 195 K in both polar regions. This occurs on average for 1 to 2 months over the Arctic but for 5 to 6 months over Antarctica (WMO, 2010). Consequently, the Arctic ozone loss is generally not as pronounced as in the Antarctic, due to the warmer temperatures inside the vortex and transport of ozone rich air into the vortex. Since the Arctic vortex is not as stable as the Antarctica vortex, it may break down and reform again several times during the cold season. As it does, warmer ozone-rich air from outside the vortex flows in leading to higher temperatures which reduce the possibility of formation of stratospheric clouds. An exception was the 2010-2011 Arctic winter when the Arctic vortex remained cold and stable over a longer period causing ozone loss comparable to that of the warmer Antarctic winters [Manney et al., 2011, Urban et al., 2011].

The following reactions describe how the ClO-dimer cycle destroys ozone in the polar vortex. The dimer was in-situ measured for the first time in the Arctic winter 2003 [von Hobe et al., 2005].

Nighttime:

$$ClO + ClO + M \underset{K_d}{\overset{K_f}{\rightleftharpoons}} Cl_2O_2 + M \tag{3.1}$$

Daytime:

$$Cl_2O_2 + h\nu \xrightarrow{J} ClOO + Cl \tag{3.2}$$

$$ClOO + M \rightarrow Cl + O_2 + M \tag{3.3}$$

$$2(Cl + O_3) \rightarrow 2(ClO + O_2) \tag{3.4}$$

$$Net : 2O_3 \rightarrow 3O_2 \tag{3.5}$$

During nighttime the catalytic dimer cycle does not take place and ClO is partitioned between monomer and dimer according to reaction 3.1. Since this reaction is temperature dependent, ClO is mostly in the form of the monomer in colder conditions and in the form of the dimer in warmer conditions. At sunrise, Cl_2O_2 is photolysed and ClO builds up quickly (reactions 3.2 to 3.4). This cycle continues in the lower stratosphere until the temperature rises (the polar vortex breaks up), the stratospheric clouds disappear and ClO_x is converted to HCl and $ClONO_2$ (deactivation). K_f and K_d represent the rate constant of reaction 3.1 in the forward and backward directions, respectively. K_f and K_d are also known as the formation rate constant and the thermal decomposition rate constant of the ClO-dimer. Photo-dissociation of Cl_2O_2 is the limiting step of the ClO-dimer cycle. In fact, the kinetic parameters of these reactions, K_{eq}= K_f / K_d and the photo-dissociation rate, J, play an important roll in the efficiency of the ozone destruction.

Generally, the ratio of ClO and its dimer from the ClO-dimer cycle can be written as:

$$\frac{[Cl_2O_2]}{[ClO]^2} = \frac{K_f[M]}{J + K_d[M]} \tag{3.6}$$

As the photolysis rate, J, is negligible during nighttime, or in other words, $J \ll K_d$, the equation can be simplified as:

$$K_{eq} = \frac{K_f}{K_d} = \frac{[Cl_2O_2]}{[ClO]^2} \tag{3.7}$$

During daytime, when $J \gg K_d$, then equation 3.6 can be simplified as:

$$\frac{[Cl_2O_2]}{[ClO]^2} = \frac{K_f[M]}{J} \tag{3.8}$$

These estimations simplify the partitioning of ClO and Cl_2O_2 at day and night. Nighttime partitioning of active chlorine is therefore controlled by K_{eq} and the daytime partitioning is governed by K_f and particularly J. In addition, the photo-dissociation of the dimer is the rate limiting step in the ClO-dimer cycle and therefore J plays a very important role in daytime partitioning.

3.2 Chlorine nighttime partitioning

As described earlier (in section 3.1), the nighttime partitioning of reactive chlorine, ClO_x, is dependent on the equilibrium rate coefficient, K_{eq}, for reactions 3.1. Calculation of ClO_x at nighttime is independent of the Cl_2O_2 photo-dissociation rate. During
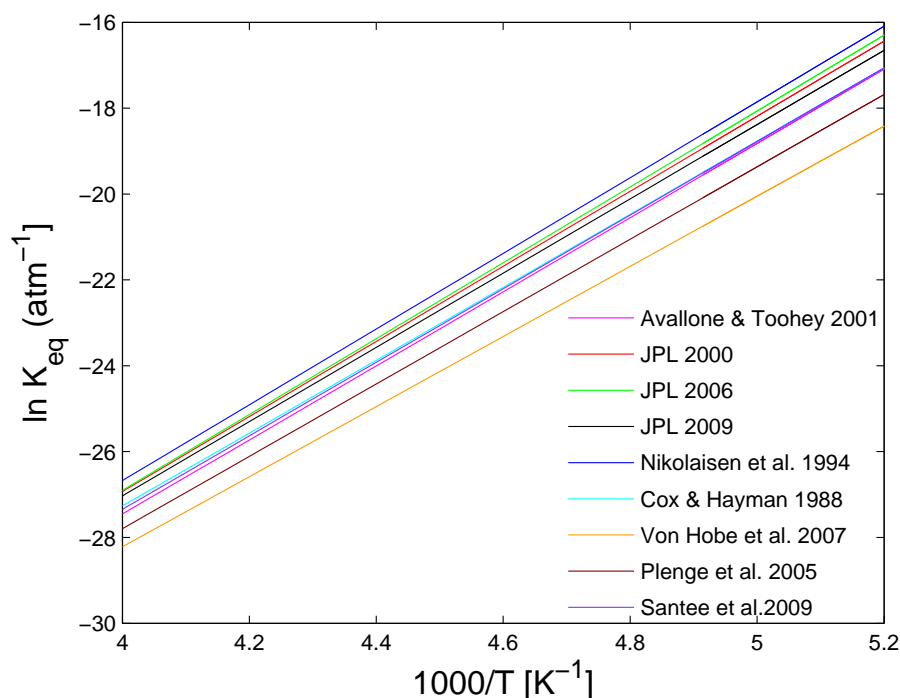
Figure 3.2: Plot showing the dependence of K_{eq} to temperature variations in the stratosphere at 20 km. Each color represents a different study for calculating K_{eq} (see legend). The blue and magenta line (Nikolaisen and Avallone-Toohey) as well as violet and cyan lines (Santee and Cox-Hayman) overlap.

night-time, the loss of ClOOCl occurs exclusively by thermal decomposition in the polar lower stratosphere. The kinetics of the reaction ClO/Cl_2O_2 during nighttime have been addressed in a number of studies [Avallone and Toohey, 2001, von Hobe et al., 2007, Cox and Hayman, 1988, Nickolaisen et al., 1994, Plenge et al., 2005, Santee et al., 2008, Sander et al., 2000, 2006, 2011]. The logarithmic presentation of the equilibrium rate constant versus temperature is depicted in Figure 3.2. The use of logarithmic scale for the figure tends to dim the divergence between different laboratory and field values. Almost all laboratory measurements of K_{eq} have been conducted at temperatures higher than those encountered in the winter lower stratosphere. This fact will increase the discrepancies between model studies. Several studies have concluded that a smaller K_{eq} than JPL recommendations should be used in models to reconcile observed nighttime ClO with model results [Stimpfle et al., 2004, von Hobe et al., 2005, Berthet et al., 2005, von Hobe et al., 2007, Schofield et al., 2008]. On the other hand, the recent JPL recommendations have been based on extrapolation of the experimental values to lower stratospheric polar temperatures. This has raised questions about the realism of the extrapolated data [Santee et al., 2010]. Therefore an accurate knowledge of K_{eq} is required to correctly estimate the partitioning of ClO and ClOOCl during nighttime and prior to sunrise.

3.3 Chlorine daytime partitioning

As described earlier, the absorption cross section defines the wavelength dependent probability of molecules for absorption and is represented in unit area (usually cm^2). The photo-dissociation of ClOOCl is the rate-limiting step in the ClO dimer cycle and also has a great influence on the rate of the ClO-BrO cycle by controlling the amount of ClO [Kurylo et al., 2009]. One of the uncertainties associated with the calculation of the photolysis rate of ClOOCl is the discrepancy between ClOOCl cross sections estimated from different experimental studies. The discrepancies in these cross sections increase for wavelengths greater than 300 nm. There have been several studies on the absorption cross section of ClOOCl, particularly for wavelengths between 250 to 350 nm. Pope et al. [2007] reported cross sections significantly lower than all reported values. Photochemical models using this cross sections underestimate the observed abundances of ClO and the ozone loss rate [von Hobe et al., 2007, Schofield et al., 2008].
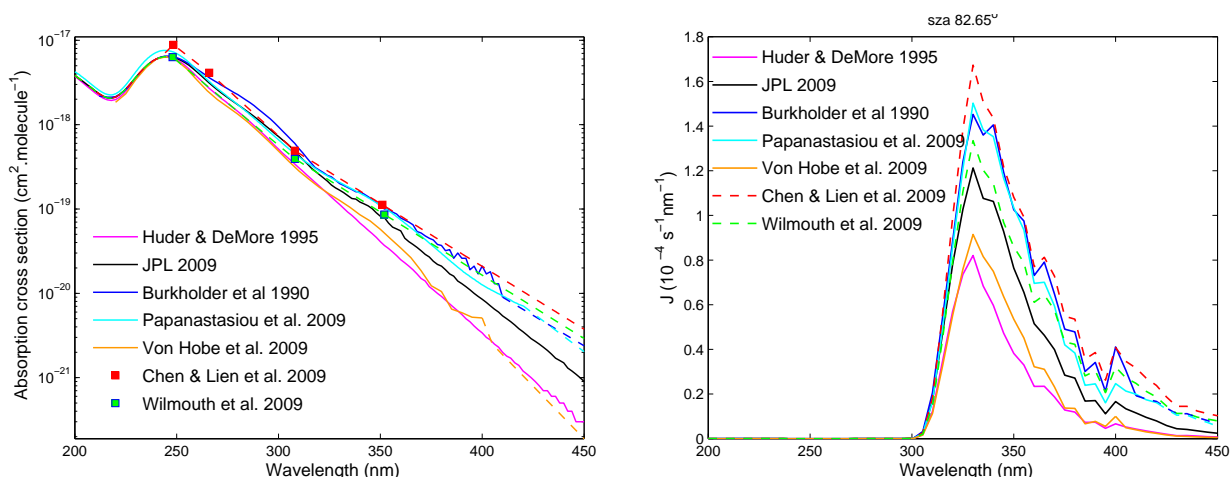
Figure 3.3: Left: Cl$_2$O$_2$ absorption cross sections versus wavelength from different laboratory studies (in logarithmic scale). The cross sections shown with solid curves are the reported values. Inter/extrapolated values between 200 to 450 nm are shown with dashed lines. The Chen et al. [2009] and Lien et al. [2009] cross sections were combined and inter/extrapolated between 248.4 to 450 nm. the Wilmouth et al. [2009] and Chen & Lien values for wavelengths lower than 248 nm are not available and JPL 2009 cross sections are used. **Right**: Corresponding photolysis rates (J values) calculated by the MISU-1D model for a solar zenith angle of 82.85^o at 20 km.

The logarithmic absorption cross sections of the ClO dimer spectrum are presented in Figure 3.3 (left). Except for the JPL2009 [Sander et al., 2009] and Huder and DeMore [1995] cross sections, we have extrapolated all cross sections log-linearly to 450 nm. Since Chen et al. [2009] and Lien et al. [2009] have used similar methods for their measurements, we have taken both cross sections together and inter/extrapolated the data between 248.4 to 450 nm. The JPL 2009 cross sections were taken for wavelengths shorter than 248.4 nm. To avoid the occurrence of sharp edges in the spectrum, the JPL cross sections between 190 to 242 nm were log-linearly extrapolated to 248.4 nm.

Wilmouth et al. [2009] reported the ClO-dimer cross sections at three wavelengths 248, 308 and 352 nm. The cross sections for wavelengths shorter than 246 nm are taken from JPL 2009 values and extrapolated log-linearly to 450 nm. The extrapolation of Burkholder et al. [1990] cross sections is somewhat uncertain due to the noise in the data, however the extrapolated data represent the overall slope and are similar to the JPL 2009 cross sections. Figure 3.3 (right) shows the photolysis rates of reaction 3.2 calculated considering the cross sections mentioned above at a solar zenith angle of 82.85^o. Chen et al. [2009] and Lien et al. [2009] values for the ClOOCl cross section give the highest photolysis rate and Huder and DeMore [1995] the lowest rate. The JPL recommendations give the photolysis rate almost in the middle (peak maximum of 1.2 s^{-1}nm^{-1}). The photolysis rate plot shows that the sensitive wavelength range of the spectrum is from 300 to 350 nm, where the peak of the photolysis rate curve is situated, and extends to 450 nm. In this region, a small change in the cross section values leads to a substantial change of the photolysis rate.

The JPL cross sections have remained unchanged from the 2006 to the 2011 recommendations (Sander et al. [2011]). JPL data are a combination of studies by Cox and Hayman [1988], Permien et al. [1988] and Burkholder et al. [1990]. Huder and De-More [1995] prepared the ClO dimer by first producing Cl_2O by oxidation of Cl_2 over HgO at low temperature and then photolysing the Cl_2O mixture. They conducted the experiment at shorter wavelengths and extrapolated the data to longer wavelengths. Their cross section results in lower values in the tail of the Cl_2O_2 spectrum (see Figure 3.3) compared with JPL recommendations. von Hobe et al. [2009] reported Cl_2O_2 cross sections smaller than JPL2009 recommendations (Sander et al. [2009]) in the range 300–350 nm. They measured the Cl_2O_2 absorption spectrum (between 220 to 400 nm) in a neon matrix at about 10 K. Instead of measuring the absolute cross sections, the cross sections were determined by scaling the measured spectrum to the peak value of the gas phase cross sections reported by JPL 2006 [WMO, 2010].

The studies of Chen et al. [2009] (308 and 351 nm) and Lien et al. [2009] (248 and 266 nm) lead to cross sections which are greater than JPL recommendations and agree more with those of Burkholder et al. [1990] and Papanastasiou et al. [2009]. Lien et al. [2009] cross sections close to the peak of the spectrum around 248.4 nm (Figure 3.3) are the highest values ever reported. Chen and Lien cross sections lead to larger photolysis rates for ClOOCl. The cross sections reported by Burkholder et al. [1990] were the highest values before Chen & Lien 2009 values were reported. Burkholder et al. [1990] produced the ClO dimer by the ClO self reaction in the gas-phase. The ClOOCl UV absorption spectrum was measured for a temperature range of 205-250 K. Wilmouth et al. [2009] formed ClOOCl using a cold temperature flowing system. Excimer lasers at 248, 308 and 352 nm photo-dissociate Cl_2O_2 and the Cl atoms are detected with atomic resonance fluorescence. Their reported values at 308 and 352 nm are in good agreement with JPL 2009 [Sander et al., 2009]. Papanastasiou et al. [2009] reported ClOOCl cross sections in the range of 300–420 nm. The spectrum peaks at 244.25 nm with cross sections greater than JPL 2009, but close to the spectrum reported by Burkholder et al. [1990] (see Figure 3.3).
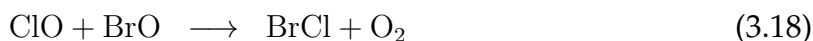
3.3.1 ClO-BrO cycle

McElroy et al. [1986] suggest that in addition to chlorine oxide radicals, bromine and chlorine oxide gas-phase reactions also contribute to polar ozone loss during winter and spring. The reaction between ClO and BrO has three pathways, leading to formation of OClO, ClOO or BrCl. The catalytic cycle involving OClO leads to a null cycle, since ozone is consumed but atomic oxygen is formed. About 60% of the reactions between ClO and BrO follow this pathway [Sander et al., 2011]:

$$ClO + BrO \quad \longrightarrow \quad OClO + Br \tag{3.9}$$
$$OClO + h\nu \quad \longrightarrow \quad ClO + O \tag{3.10}$$
$$Br + O_3 \quad \longrightarrow \quad BrO + O_2 \tag{3.11}$$
$$Net: O_3 \quad \longrightarrow \quad O_2 + O \tag{3.12}$$

However, the two other pathways lead to ozone loss cycles. The pathway generating ClOO (about 32%) initiates the following cycle:

$$ClO + BrO \quad \longrightarrow \quad ClOO + Br \tag{3.13}$$
$$ClOO + M \quad \longrightarrow \quad Cl + O_2 + M \tag{3.14}$$
$$Br + O_3 \quad \longrightarrow \quad BrO + O_2 \tag{3.15}$$
$$Cl + O_3 \quad \longrightarrow \quad ClO + O_2 \tag{3.16}$$
$$Net: 2O_3 \quad \longrightarrow \quad 3O_2 \tag{3.17}$$

The pathway giving BrCl and accounts about 8% of the overall ClO-BrO reactions [Sander et al., 2011]:

$$ClO + BrO \quad \longrightarrow \quad BrCl + O_2 \tag{3.18}$$
$$BrCl + h\nu \quad \longrightarrow \quad Cl + Br \tag{3.19}$$
$$Br + O_3 \quad \longrightarrow \quad BrO + O_2 \tag{3.20}$$
$$Cl + O_3 \quad \longrightarrow \quad ClO + O_2 \tag{3.21}$$
$$Net: 2O_3 \quad \longrightarrow \quad 3O_2. \tag{3.22}$$

The contribution of ClO+ BrO cycles in the Arctic lower stratospheric ozone destruction is estimated to be about 25%, while ClO-dimer cycles account for about 75% of the total ozone loss in this region [Pfeilsticker et al., 2000].

3.4 Simulating polar disturbed chemistry

3.4.1 General consideration

The MISU-1D model does not include transport processes. However, since the model is applied for the condition of the Arctic lower stratosphere where the life-times of ClO_x and BrO_x are much shorter than the transport time-scale, this deficiency does not affect the results significantly. Air inside the Arctic polar vortex is isolated from

Date of flights	Transition	Latitude	Longitude
2 March 1996	Night-Day	70^oN – 69.7^oN	3^oE – 21^oE
25 February 1997	Day-Night	69.9^oN – 69.1^oN	11^oW – 24^oE
23 January 2000	Night-Day	72^oN – 63^oN	10^oE – 19^oE

Table 3.1: List of ASUR flights providing observations of ClO across the terminator.

the surrounding air during the winter and beginning of spring. In cold Arctic winters (temperatures below 195 K) polar stratospheric clouds are formed and chlorine and bromine species are converted to their reactive forms. Therefore, ozone chemistry in twilight condition is controlled almost exclusively by the ClO-dimer and ClO-BrO catalytic cycles (reactions 3.1 to 3.4 and reactions 3.9 to 3.21). Accordingly, the assumption of considering only these two cycles in perturbed chemistry conditions makes sense, provided that ClO_x and BrO_x are initialized with elevated concentrations which are observed typically in the polar lower stratosphere under perturbed conditions and the ozone concentration is fixed to the values obtained from observations. The model is initialized with ClO_x (defined as [ClO] + 2[Cl_2O_2]+[Cl]) and BrO_x ([BrO]+[Br]). The other chlorine and bromine species are initialized to zero. The photolysis rates (J) of the ClO-dimer (reaction 3.2) and the equilibrium rate constants of reaction ClO/ClOOCl define the partitioning of active chlorine species in the model. The full diurnal cycle with a variable sun position during the course of a day is simulated with the calculation of J values updated at each time step in the solver (every 3 minutes). The model is also constrained using observed values of temperature and pressure and takes overhead ozone and albedo into account.

3.4.2   Comparison with ASUR observations

ASUR (Airborne SUbmillimeter Radiometer) is a sub-millimeter heterodyne radiometer measuring ClO thermal emission spectra at about 650 GHz [Urban, 1998]. ASUR measures ClO, HCl, N_2O and other trace gases in an altitude range of 15-50 km. The vertical resolution is typically 6–10 km. In this study, simulations were performed in order to compare the model with ClO observations retrieved from ASUR airborne measurements on 2 March 1996, 25 February 1997 and 23 January 2000. Table 3.1 shows information about the ASUR observations and the geographical positions of the airplane at an altitude of 20 km. For this study, we used ClO reanalyzed measurements (see paper I for details) in order to assume that all flights (from thre different campaigns) are treated equally.

The ozone profile for the MISU-1D simulations is taken from ozone-sonde measurements conducted in the Arctic vortex (Sodankylä, 67.4^oN/26.6E^o) [Kivi et al., 2007]. The ozone profile is used as input for the calculation of the optical depth in the atmosphere. The absorption cross sections and reaction rates are taken from the standard JPL 2009 recommendations [Sander et al., 2009] shown in section 3.2 and 3.3. The simulations have been performed for conditions of the locations of the measurements. This means

that the length of the day and sunrise/sunset changes in the model correspond to the latitudes of the measurements. The BrO_x profile is taken from balloon-borne measurements conducted over Kiruna, Sweden (68^oN, 21^oE), in February 1999 [Pfeilsticker et al., 2000]. The model calculates the temporal development of chlorine monoxide during 24-hours using the results of the previous simulation to initialize the following 24-hour simulation.
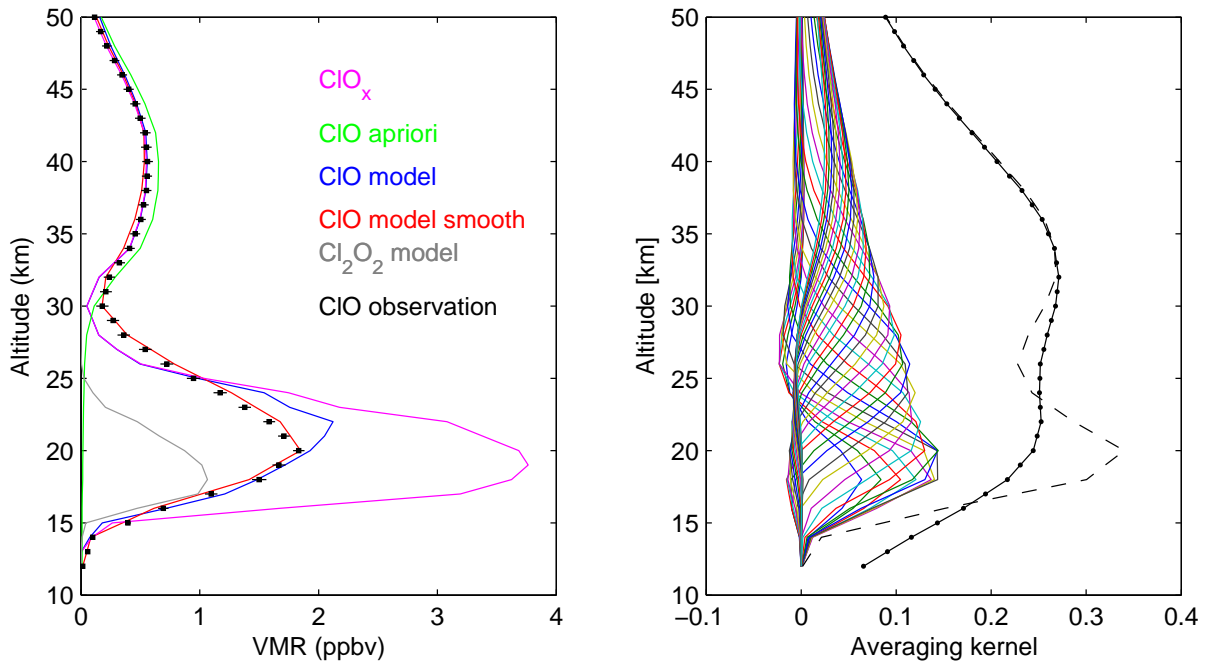
Figure 3.4: Left: Model profiles of ClO_x, Cl_2O_2 and ClO (unconvolved and convolved) in volume mixing ratio compared to ClO observations from ASUR on 23 January 2000 (at $\sim63.1^oN$ and a solar zenith angle of $\sim83.1^o$ which corresponds to noontime), along with the ClO apriori profile used by the retrieval algorithm. The error bars represent the statistical errors of the measurement. Right: Averaging kernel matrix from ASUR. Dashed lines are the sum of the kernel matrix rows and dotted lines are the sum of the kernel matrix columns, both divided by 4 for better visualization.

To account for the limited vertical resolution of the measurements, the model ClO results were smoothed using the ASUR apriori information and averaging kernel functions following the method described by Connor et al. [2007]. This ensures us that any departure of the model from the measurement can not be due to the unequal vertical resolution. The model produces higher resolved profiles for each species and should be degraded to the measurement resolution. The peak of each averaging kernel provides information about the altitude of maximum sensitivity of the observation. For all simulations, the same apriori profile and averaging kernel have been used.

$$ClO_{smooth} = ClO_{apriori} + A * (ClO_{model} - ClO_{apriori}) \qquad (3.23)$$

A and $ClO_{apriori}$ are the low resolution averaging kernel matrix and apriori profile,

respectively. The apriori profile is our reference profile and is generally a climatological estimation of the measured species vertical profile. The sum of the rows of the averaging kernel matrix represents the measurement response. The measurement response determines the best altitude range (values close to unity) at which the majority of the information comes from the measurement rather than from the a priori. Figure 3.4 shows an example of ASUR averaging kernels which are used for vertical smoothing of the simulated ClO profiles. The vertical resolution of the kernel peaked at 20 km is about 7–8 km, which is the full width at half maximum of the kernel at this level.

The ASUR measurement flights in March 1996 and February 1997 were carried out along almost constant latitudes, namely from 70° to 69.7^o and 69.9^o to 69.1^o for observations at 20 km. The corresponding model simulations were conducted for calculations of a mean latitude of 69.8^o and 69.3^o, respectively. The January 2000 flight was carried out across latitudes from 71.12^o to 63.12^o. The simulations were then done at each latitude of the individually defined ClO profiles and then reassembled to construct the observed diurnal variations. The ClO measurements and simulations are presented in Figure 3.5. The Figures show the ClO measurements of ASUR for the three flights of March 1996, January 2000 and February 1997. The first two measurements (left and middle) are night-day flights, whilst the right plot shows a day-night transition flight. The ClO abundance does not exceed 1.1, 1.8 and 1 ppbv, respectively, with a peak at roughly 20 km. The figures in the middle row represent the ClO model calculations based on JPL 2009 recommendations for both K_{eq} and ClOOCl cross sections. The smoothed model results are presented in the last row of the figure. The smoothed model results agree with the measurements between 12 to 30 km with excellent agreement in daytime. Nighttime calculations are higher than the observations for all the observations. The modelled and vertically smoothed ClO profiles were compared and ClO_x in the model was chosen to match the measured ClO at the lowest solar zenith angles of the field observations.

3.5 Results

The model results show the temporal development of chlorine monoxide in terms of volume mixing ratio (ppbv) at 20 km compared with air-borne observations (ASUR). Since the concentration of ClO is strongly dependent on the solar radiation, its mixing ratios are plotted versus solar zenith angle which is a measure of the intensity of solar radiation. The solar zenith angles larger than $\sim 93^o$ represent nighttime and those smaller than 90° represent daytime. The kinetics of the reactions contributing to the diurnal variation of ClO (photolysis rate which is a function of photo-dissociation cross sections of the ClO-dimer and thermal equilibrium rate constant of nighttime partitioning) are tested. These kinetics determine the partitioning of ClO during the course of a day. The uncertainties of the model result to parameters such as temperature and albedo are presented. Temperature affects the equilibrium rate constant of the ClO/ClOOCl reaction (Arrhenius expression) and albedo affects the amount of radiation received by an atmospheric layer. In addition, the influence of ClO-BrO reaction
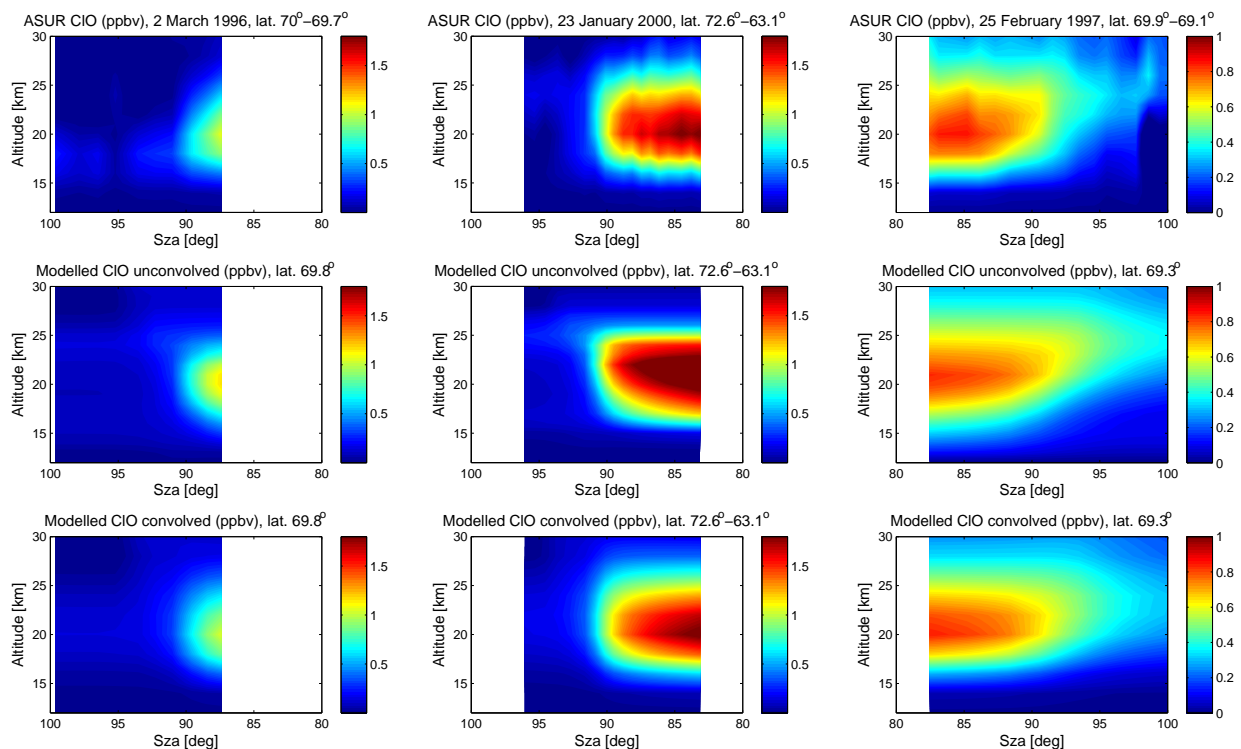
Figure 3.5: Top row: ClO measurements made by ASUR on 2 March 1996 (left, night-day flight), on 23 January 2000 (middle, night-day flight) and on 25 February 1997 (right, day-night flight). ClO volume mixing ratios are shown in ppbv. **Middle row**: Model simulations (both ClOOCl cross sections and K_{eq} are according to JPL 2009 recommendations). Simulations on January 2000 were carried out for a latitude range of 72.6^o to 63.12^o corresponding to the measurements. Simulations on March 1996 and February 1997 were conducted for fixed latitudes of 69.8^o and 69.2^o, respectively. **Bottom row**: Same simulations as the middle row, but convolved with ASUR averaging kernels in order to account for the limited altitude resolution of the measurements.

cycle on the ClO diurnal variation is also tested. The results are presented in the following sections.

3.5.1 Sensitivity of the ClO calculation to the Cl_2O_2 cross section

The sensitivity of the ClO diurnal variation to the ClOOCl cross sections at 20 km is presented in Figure 3.6. Here the cross sections shown in Figure 3.3 were used in the model runs. The error bars are the 1-σ statistical error of the ASUR ClO observations. As can be seen, changing the cross sections only changes the amount of ClO during daytime. The Chen & Lien [Chen et al., 2009, Lien et al., 2009] cross sections reproduce higher model daytime ClO, while Huder and DeMore [1995] cross sections give the lowest ClO. Total active chlorine, ClO_x, is calculated using the JPL 2009 [Sander et al., 2009] cross sections and equilibrium rate constant K_{eq} (black curves, Figure 3.7). An uniform chlorine activation is assumed along the flight track, i.e. the ClO_x profile does
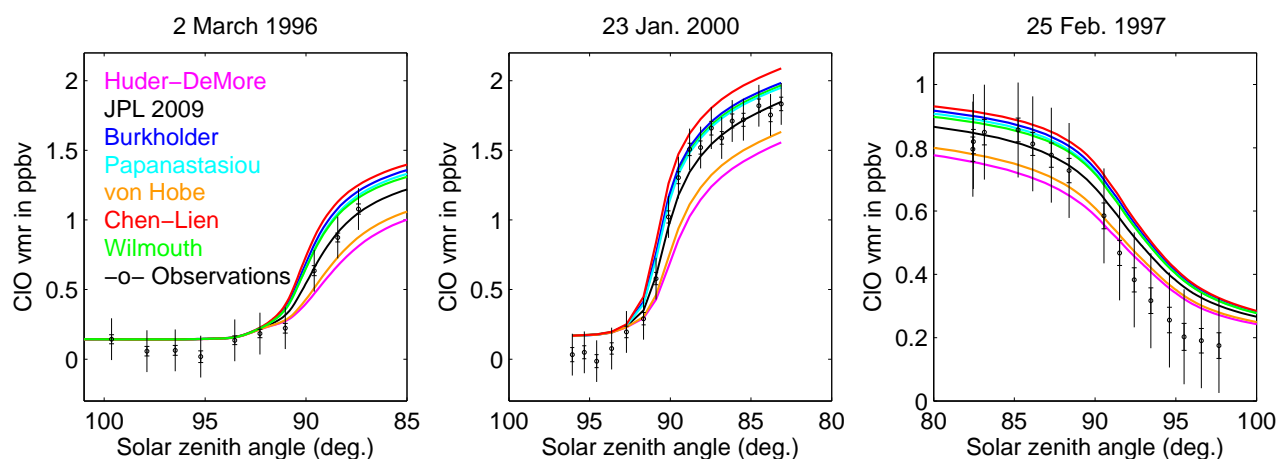
Figure 3.6: ClO diurnal variation simulations using different ClOOCl cross sections (see legend) and comparison with field observations on March 1996 (left), 23 January 2000 (middle) and 25 February 1997 (right). The smaller error bars show the 1-σ statistical error and the larger ones represent the systematic errors (10% or 0.15 ppbv, whatever is larger) in the observed values [Kleinböhl, 2004, von König, 2001]. The total active chlorine in the model is tuned to the observations at low solar zenith angles assuming the JPL 2009 cross section and equilibrium rate constant.

not vary between latitudes.

In the next step, the simulations have been optimized by using different ClO_x profiles for initialization (Figure 3.8). To verify which cross sections can be reconciled with the observations, the initial ClO_x has been calculated so that it produces the same daytime ClO as the field measurements. The ClO_x profiles are shown in Figure 3.7. Accordingly, the simulations (January 2000 and March 1996) using smaller ClOOCl cross sections [Huder and DeMore, 1995, von Hobe et al., 2009] need to be initialized with larger active chlorine (about 3.7 ppbv and higher, according to Figure 3.7), while those simulations using larger cross sections such as Chen & Lien [Chen et al., 2009, Lien et al., 2009] or Papanastasiou et al. [2009] values can be initialized with smaller values (below 3.4 ppbv, Figure 3.7).

The upper limit for ClO_x is restricted by the total inorganic chlorine, Cl_y, plotted in Figure 3.7 (see **paper I**). The JPL 2009 [Sander et al., 2009], von Hobe et al. [2009] and Huder and DeMore [1995] cross sections, especially for the January 2000 flight when the conditions were close to full chlorine activation (very low HCl mixing rations around 18-20 km altitude), require unrealistic high ClO_x (3.7, 4.6 and 5.1 ppbv) which exceeds Cl_y and therefore do not allow us to reconcile the model with the observations. ClO_x profiles estimated for the March 1996 flight also exceed Cl_y (3.5 and 4.1 ppbv), when applying von Hobe et al. [2009] and Huder and DeMore [1995] cross sections despite less chlorine activation observed in March 1996. The model matches ASUR observations during daytime applying cross sections leading to faster photolysis rates [Wilmouth et al., 2009, Papanastasiou et al., 2009, Burkholder et al., 1990, Chen et al., 2009, Lien et al., 2009].
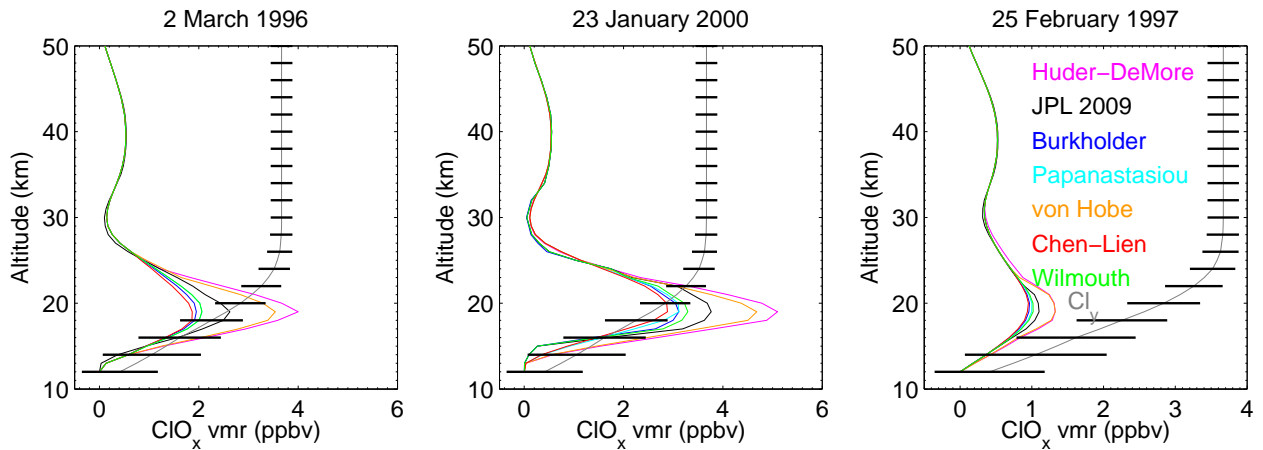
Figure 3.7: The optimized total active chlorine ClO_x assumed for the model runs. Cl_2O_2 cross sections derived from several studies were used (see legend). Simulations are for 2 March 1996 (left), 23 January 2000 (middle) and 25 February 1997 (right). In the left plot, ClO_x estimated for Papanastasiou et al. [2009] cross sections (in cyan) is covered by ClO_x estimated for Wilmouth et al. [2009] (in green). In the right plot, ClO_x estimated for Huder and DeMore [1995] (in magenta) has been covered by von Hobe et al. [2009] (orange) and ClO_x for Chen et al. [2009], Lien et al. [2009] also overlaps Burkholder et al. [1990] as well as ClO_x for Papanastasiou et al. [2009] overlapls Wilmouth et al. [2009]. The gray line with black error bars is the Cl_y estimated profile for paper I.
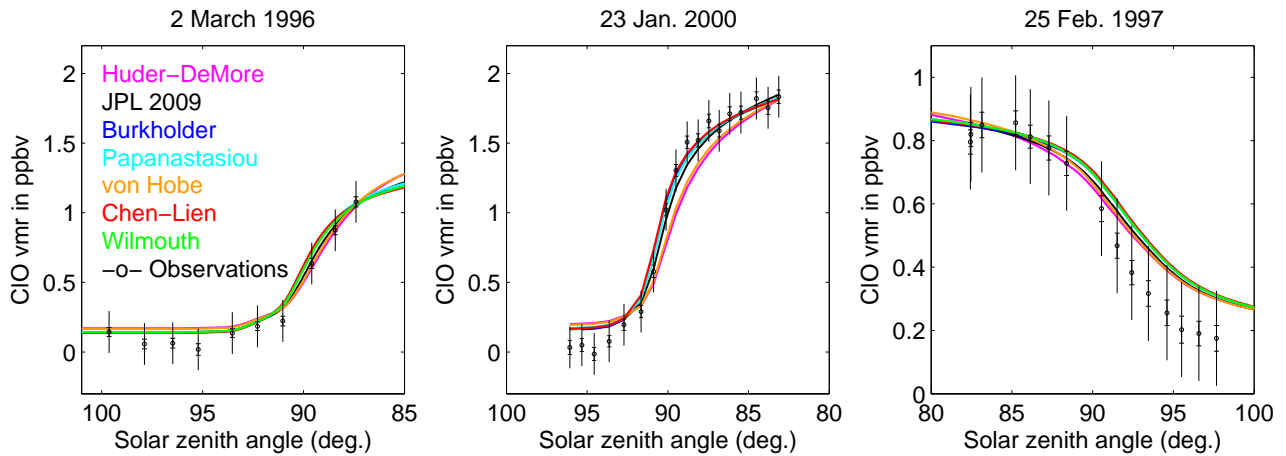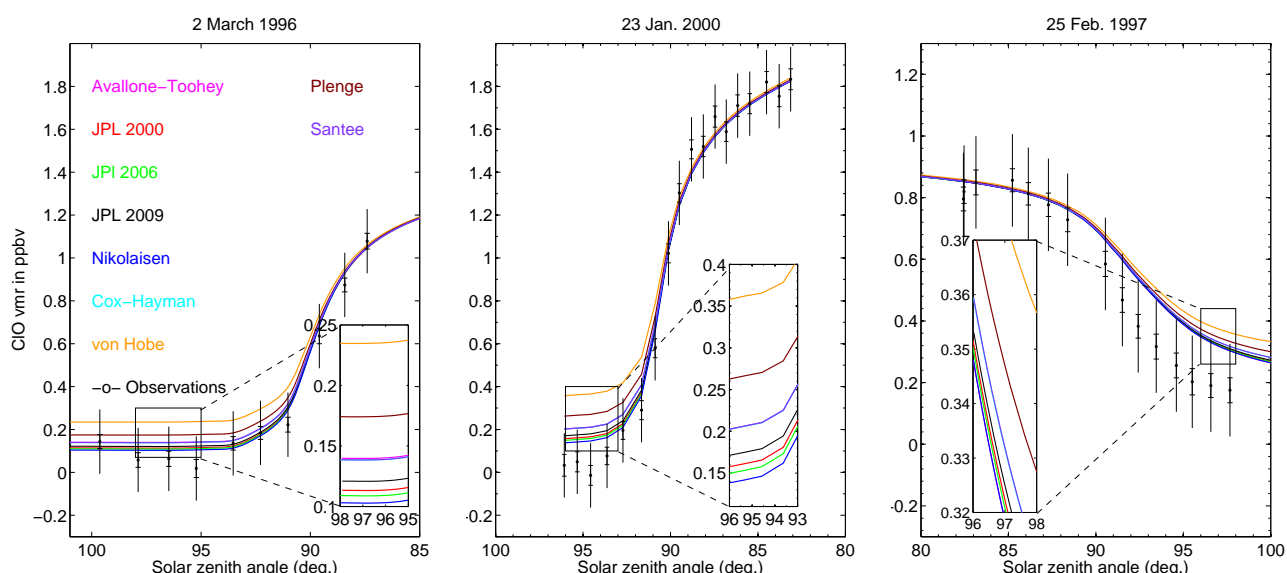

Figure 3.8: Simulated ClO diurnal variations using different ClOOCl cross sections (see legend) with the ClO_x according to the optimized profiles in Figure 3.7 and comparison with field observations on March 1996 (left), 23 January 2000 (middle) and 25 February 1997 (right). The smaller error bars show the 1-σ statistical error and the larger ones represent the systematic errors (10% or 0.15 ppbv, whatever is larger) in the observed values (paper I).

The results of our study are consistent with previously reported studies. von Hobe et al. [2007] reported that Huder and DeMore [1995] cross sections are too low to be consistent with atmospheric observations. von Hobe et al. [2007] also discussed that studies by Chipperfield et al. [2005], Tripathi et al. [2006], Frieler et al. [2006] show that models using the ClO-dimer cross sections lower than JPL 2006 underestimate

the ozone loss and that using the higher Burkholder et al. [1990] cross sections gives the best agreement of the modelled ozone loss with observations. Sumińska-Ebersoldt et al. [2012] reported that their observation of daytime ClO is consistent with cross sections higher than those published by von Hobe et al. [2009] and lower than those published by Papanastasiou et al. [2009]. Note that, Sumińska-Ebersoldt et al. [2012] have scaled the von Hobe et al. [2009] cross sections at the peak of the spectrum to the values reported by Lien et al. [2009] which has increased the photolysis rate of the dimer. The new version of JPL [Sander et al., 2011] recommends using the Papanastasiou et al. [2009] cross sections which is consistent with our results.

3.5.2 Sensitivity to K_{eq}

In this section, ClO nighttime calculations based on different thermal equilibrium rate constants, K_{eq}, from several studies have been compared with observations to test the consistency of the model with the observations. The result is presented in Figure 3.9.

Figure 3.9: Model ClO diurnal variation in volume mixing ratio assuming different K_{eq} (see legend) and ASUR observations. The absorption cross sections in these simulations are according to the JPL 2009 recommendation and the ClO_x profiles are according to the black curves in Figure 3.7. The simulations using Santee and Cox-Hayman (violet and cyan) as well as simulations with Nikolaisen and Avallone-Toohey (blue and magenta) overlap. Nikoaisen and Avallone-Toohey line are the lowest and Santee and Cox-Hayman in the middle. The smaller error bars show the 1-σ statistical error and the larger ones represent the systematic errors (10% or 0.15 ppbv, whatever is higher) in the observed values (paper I). **Left**: 2 March 1996, **Middle**: 23 January 2000. **Right**: 25 February 1997.

Figure 3.9 shows the sensitivity of the ClO abundances to various recommendations for calculation of K_{eq}. The assumed total active chlorine is according to the the profiles in Figure 3.7 for Papanastasiou et al. [2009] cross sections. All values of K_{eq} adopted

for the simulations lead to an overestimation of the nighttime ClO. This can be observed most obviously in the February 1997 and January 2000 simulations. The model calculates about 0.07–0.3 ppbv and 1.2–0.2 ppbv higher nighttime ClO compared with the mean of nighttime observations in night-day and day-night simulations, respectively. Among different parametrization of K_{eq}, the Nickolaisen et al. [1994], Avallone and Toohey [2001] and JPL 2000 to JPL 2009 parameterizations give the lowest ClO at high solar zenith angles, while von Hobe et al. [2005] and Plenge et al. [2005] give the highest ClO. The simulations using Santee et al. [2010] and Cox and Hayman [1988] are between the simulation using Plenge et al. [2005] and JPL 2009 [Sander et al., 2009]. The analysis of night time ClO reported by Berthet et al. [2005] also concludes that the introduction of K_{eq} given by von Hobe et al. [2005] at temperatures below 220 K leads to an overestimation of ClO in their model. They suggest an estimation of K_{eq} between the values determined by Cox and Hayman [1988] and the values suggested by von Hobe et al. [2005]. Since the model generally calculates higher nighttime ClO than the observations, it is difficult to conclude which K_{eq} gives consistent results with the measurement. However simulations based on von Hobe et al. [2005] and Plenge et al. [2005] give nighttime ClO which is above the upper uncertainty range of the observations. The results of our study agrees with Sumińska-Ebersoldt et al. [2012] which conclude that their result is not consistent with equilibrium constants higher than the one proposed by Plenge et al. [2005].

3.5.3   Temperature sensitivity

The sensitivity of the model calculation of ClO to temperature within the uncertainty range of $T_{mean} \pm 2$ K was investigated in order to test how the model results might be influenced by uncertainties in the assumed temperature profile. The results were compared with the observations performed on 2 March 1996, 23 January 2000 and 25 February 1997. Figure 3.10 shows the difference between the model calculation of ClO using the higher and lower temperature uncertainty and the model using the mean temperature. The temperature data used for the ASUR analysis are taken from the National Centers for Environmental Prediction (NCEP) analysis for the period and location of the observations. An uncertainty in the temperature profiles can lead to some variations in the amount of ClO calculated by the model. The result shows that higher temperatures shift the model simulations towards more ClO during day and night. The ClO simulations for 2 March 1996 and 23 January 2000 show the highest sensitivity to temperature as the ClO changes by about 0.025–0.035 ppbv for the lowest (T_{mean}-2 K) and by about 0.03–0.04 ppbv for the highest temperatures (T_{mean}+2 K). The temperature variability has a smaller effect on the day-night transition of ClO. The simulations on February 1997 show maximum changes of 0.02 ppbv at high solar zenith angles (∼10%). Warmer temperatures shift the ClO/Cl_2O_2 thermal equilibrium towards less dimer formation. The lower nighttime ClO can not be modeled by taking into account the 2 K temperature uncertainties. Eyring [1999] have also used ASUR ClO observed on 2 March 1996 and 25 February 1997 from an older retrieval algorithm [Urban, 1998] and compared to the results from new model study. She concludes that the nighttime ClO can not be modeled by taking temperature uncertainties of 5 K into account which

is consistent with this study.
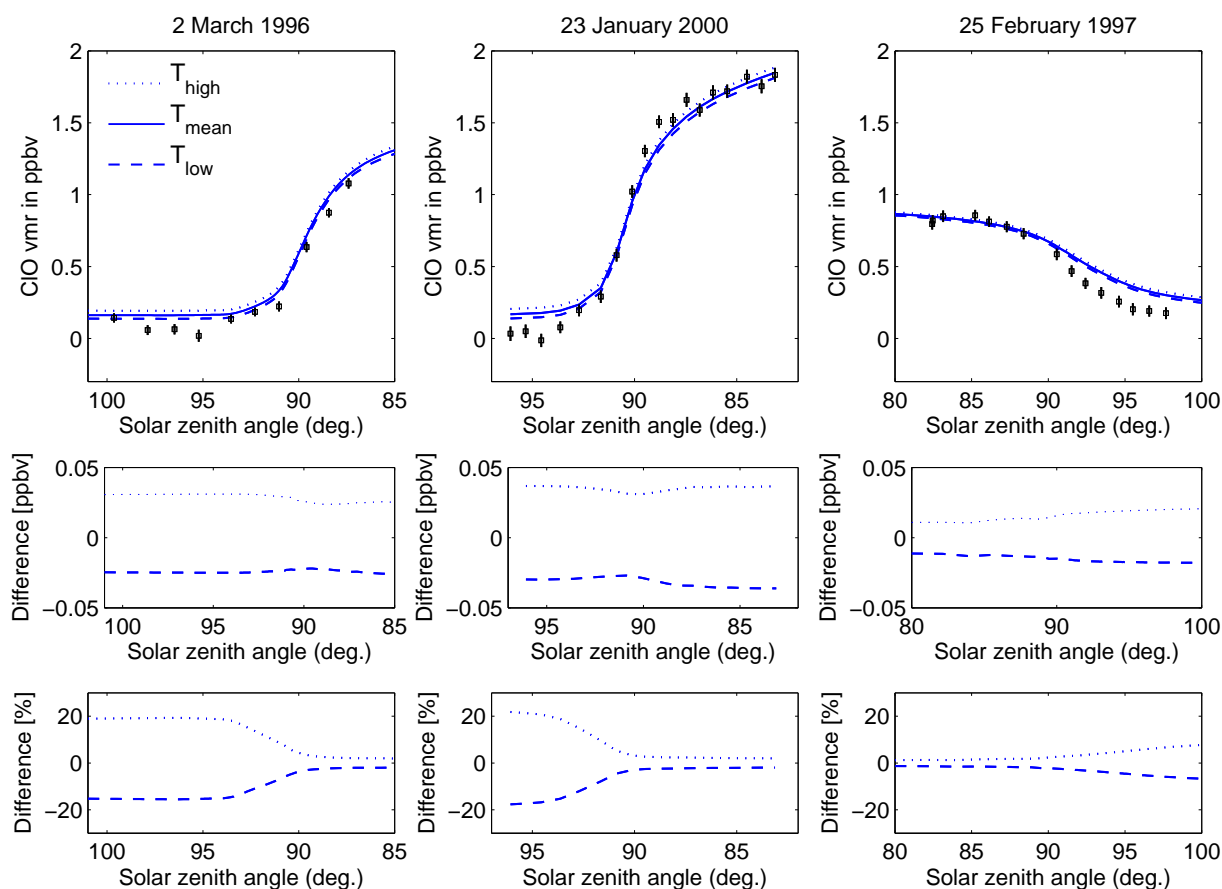
Figure 3.10: Top row: Model calculation of the ClO diurnal variation (in VMR) at 20 km using a 2 K temperature uncertainty and comparison with field observations on March 1996 (left), 23 January 2000 (middle) and 25 February 1997 (right). The total active chlorine, ClO_x, in the model is tuned for all the simulations to give similar ClO at the daytime measurement points with lowest solar zenith angle. The simulations assume JPL 2009 cross sections and equilibrium rate constants. **Middle row**: Difference between the model using the mean temperatures and the perturbed temperatures. **Bottom row**: Differences as percentages.

3.5.4 Albedo sensitivity

The albedo is an important factor controlling the amount of radiation received by each atmospheric layer. Higher albedo increases multiple scattering and radiance. This increases the photo-dissociation of the ClO-dimer at dawn and dusk. Figure 3.11 shows the effect of changing the albedo between 0 and 0.1 on the ClO modelled in twilight conditions. The measurements were carried out mostly above the open water, where the albedo is very low and close to zero. The effect of albedo is most visible at sunrise and sunset at solar zenith angles of about 90°–97°. An albedo of 0.1 leads to an increase of ClO around sunrise by up to 0.07 ppbv (38%) and around sunset by up

40

to about 0.05 ppbv (17%) compared with model runs using albedo 0, for the here discussed simulations and assumed amount of activated chlorine and bromine. Higher albedo would thus cause even higher ClO in the model and would not lead to better agreement with the measurements which suggest lower mixing ratios. This result for the albedo sensitivity is consistent with the study by Wetzel et al. [2012] who claim that surface albedo and tropospheric clouds do not change the photolysis of ClOOCl and the ClO abundance significantly. Wetzel et al. [2012] also conclude that polar stratospheric clouds may lead to a delayed ClO formation around sunrise by reducing the direct radiative flux from the sun. The results of our model study do not indicate any delay which could be due to the presence of polar stratospheric clouds.
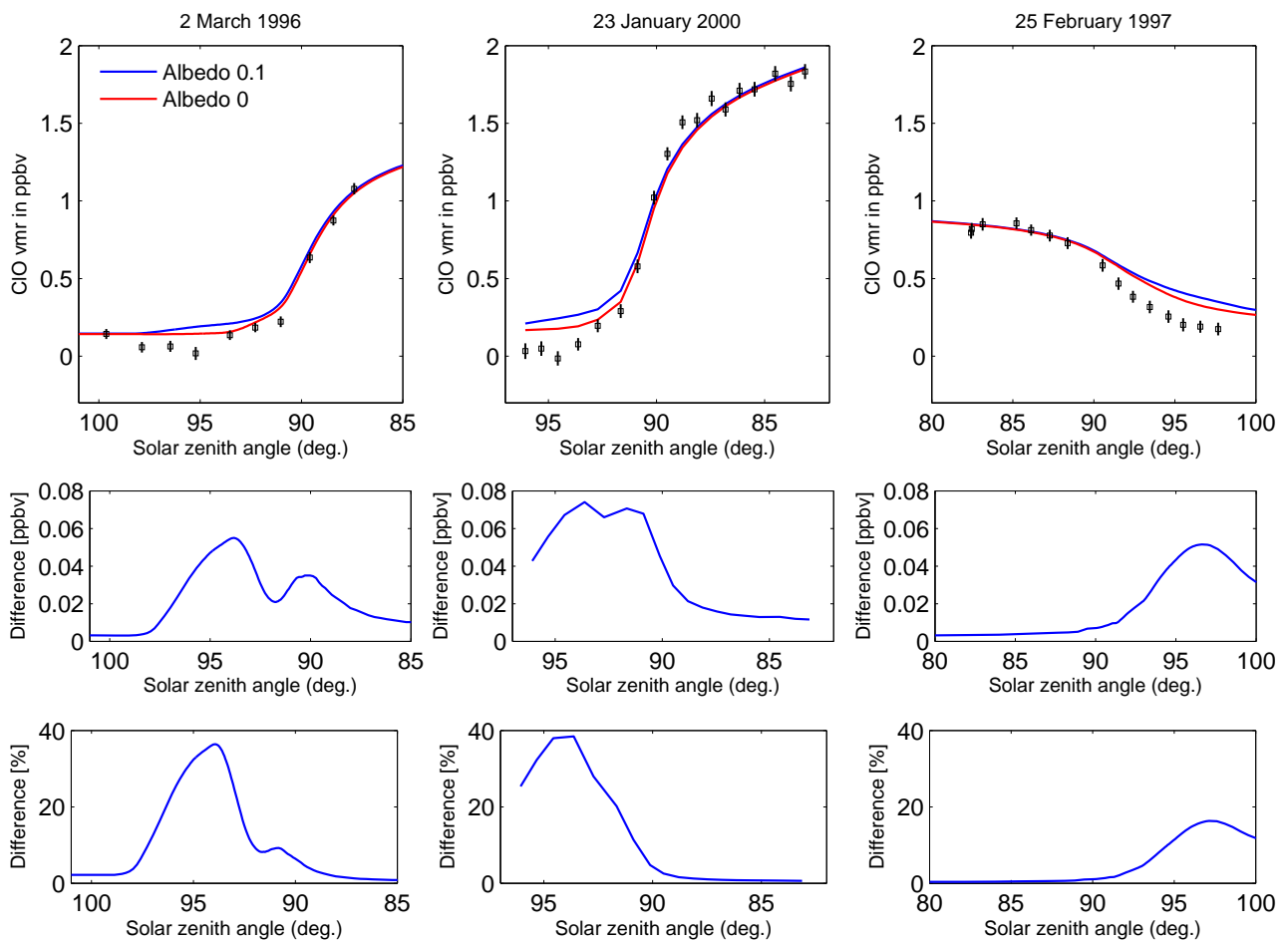
Figure 3.11: Top row: Model calculation of the ClO diurnal variation (in VMR) at 20 km using albedos of 0 and 0.1 compared with field observations on March 1996 (left), 23 January 2000 (middle) and 25 February 1997 (right). The total active chlorine, ClO_x, in the model is tuned to give the same ClO at the last daytime measurement points assuming JPL 2009 cross sections. **Middle row**: Difference between two model runs applying albedo 0 and 0.1. **Bottom row**: Differences shown as percentages. simulations with albedo 0 are taken as references.

3.5.5 Influence of ClO-BrO cycle
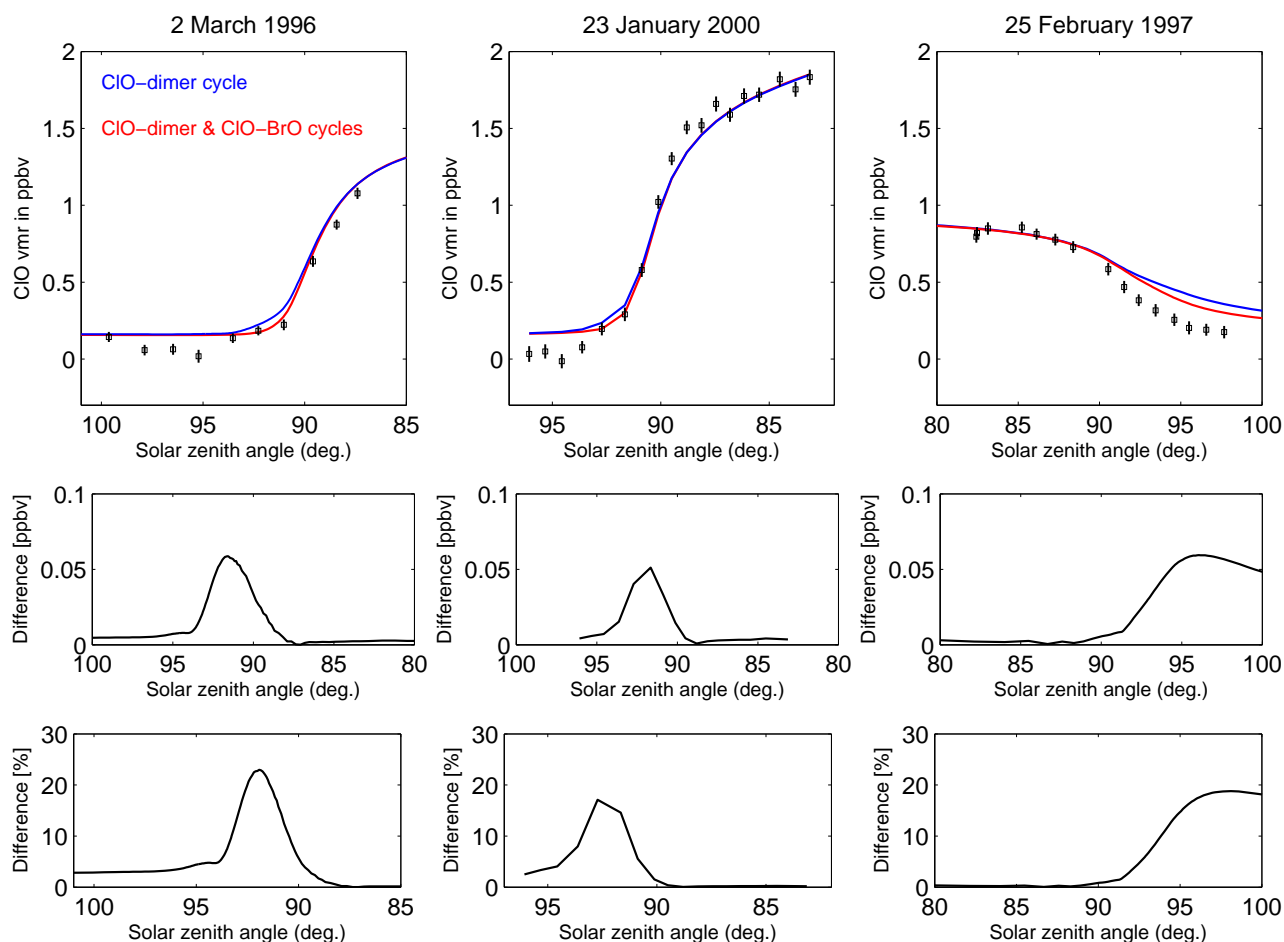
Figure 3.12: Top row: Model calculation of the ClO diurnal variation (in VMR) at 20 km. Comparison of simulations with only the ClO-dimer cycle and simulations with the ClO-dimer plus the ClO-BrO cycle. Field observations for 2 March 1996 (left), 23 January 2000 (middle) and 25 February 1997 (right) are also shown. The total active chlorine, ClO_x, in the model is tuned for all the simulations to give the same ClO at the daytime measurement points with the lowest solar zenith angle. **Middle row**: Absolute differences between the simulations using only the ClO-dimer cycle and the simulations with the ClO-BrO and ClO-dimer cycles at 20 km. **Bottom row**: Relative differences between the two simulations when the simulation with both cycles is considered as reference.

BrO is formed by the reaction of Bromine atoms realease by the photolysis of bromine-contained species in the stratosphere. The ClO-BrO cycle accounts for about 25% of the ozone loss in the lower stratosphere, while the ClO-dimer cycle stands for about 75% of the ozone loss [Pfeilsticker et al., 2000, Finlayson-Pitts and Pitts, 1999]. In this section, the sensitivity of the ClO diurnal variation to the ClO-BrO cycle is investigated and the results are illustrated in Figure 3.12. Inclusion of the ClO-BrO reactions does not change the ClO concentrations significantly during day and night, but ClO changes up to 0.05 ppbv (17–23%) around sunrise and sunset (solar zenith angles 90°–95°) for the here considered ClO_x and BrO_x amounts. ClO observations drop faster than the

modelled ClO in 25 February 1997 at solar zenith angles above 105°. Eyring [1999] reported consistently that the simulated ClO at solar zenith angles ranging from 90°–100° increases by up to 14% when ClO-BrO reaction cycles are excluded compared to simulations with full chemistry . In this study we found similar result for the day-night simulations (25 February 1997) as the ClO-BrO cycle lowered ClO by up to 18% in the same range of solar zenith angles. Note that the BrO_x profile used for the initialization of the model was calculated for January 2000 with a full chlorine activation and it is used for the initialization of the simulations on February 97 and March 96 as well. This will add to the uncertainty of the simulations.

BrO is built up during daytime similar to ClO and thus has minimum values at night. BrCl is the nighttime reservoir and is photolysed during the day. Consequently the probability of the reaction between BrO and ClO increases after sunrise. ClO is found in higher concentrations than BrO and the reaction between these species can not change the daytime ClO extensively. During the sunrise and sunset, however, the two molecules are formed or lost quickly and the ClO-BrO reactions have more effect on the ClO abundance.

3.6 Conclusions (study I)

The main findings of this study can be summarized as:

- Cl_2O_2 cross sections:

  The combined Chen & Lien [Chen et al., 2009, Lien et al., 2009] Cl_2O_2 cross sections lead to highest model ClO during daytime, while Huder and DeMore [1995] cross sections give the lowest ClO. The MISU-1D model simulates a very similar shape of the diurnal variation behavior of ClO as the ASUR measurements once the available ClO_x is properly adjusted. The model agrees best with ASUR observations applying Cl_2O_2 cross sections of Wilmouth et al. [2009], Papanastasiou et al. [2009], Burkholder et al. [1990] and Chen & Lien [Chen et al., 2009, Lien et al., 2009], which all lead to fast photolysis of ClOOCl. Model results using smaller cross sections from Huder and DeMore [1995] and von Hobe et al. [2009] (and to a lesser extent from JPL 2009 [Sander et al., 2009]) can not be reconciled with the ASUR observations, since these would require ClO_x values exceeding available Cl_y. Our result supports the new JPL recommendations [Sander et al., 2011] which is based on the fast Papanastasiou et al. [2009] cross sections.

- Equilibrium rate constant:

  The MISU-1D model calculates higher nighttime ClO compared to the ASUR observations for all tested K_{eq}, applying the ClO-dimer photolysis cross sections according to Papanastasiou et al. [2009] recommendations. This difference is more pronounced for the day-to-night simulations, as ClO concentrations do not drop

with the same rate (slope) as the observations do. Due to the considerable systematic uncertainty of the measurements (of 0.15 ppbv), it is difficult to conclude which K_{eq} gives consistent results. However simulations based on von Hobe et al. [2005] and to a lesser extent Plenge et al. [2005] give too high nighttime ClO.

- Model uncertainties:

  Temperature uncertainties affect modelling of the ClO diurnal cycle. Applying a 2 K temperature variation alters the absolute ClO by up to ∼0.04 ppbv for the cases considered here. The observed higher nighttime ClO can therefore not be reproduced by the model considering the temperature uncertainty.

  Higher albedo increases multiple scattering and radiances and consequently the photo-dissociation of the ClO-dimer. Modelled ClO is mainly sensitive to the albedo around sunrise and sunset. For the simulations and observations discussed here, using an albedo of 0.1 gives about 0.07 and 0.05 ppbv higher ClO at sunrise and sunset, respectively, compared to the model runs using albedo 0. As for the temperature uncertainty, the albedo uncertainty does not allow us to reconcile the higher model nighttime ClO with the measurements.

- Contribution of BrO-ClO cycle:

  The ClO-BrO reaction cycle decreases ClO around sunrise and sunset by up to about 0.05 ppbv, but does not change the ClO concentrations significantly during day and night. The results are consistent with earlier findings by Eyring [1999].

Chapter 4

Study II: Short-lived species in the tropical stratosphere

This chapter describes the partitioning of the chemical species and their diurnal variation in the tropical stratosphere and lower mesosphere region based on calculations with the MISU-1D photochemical model. The modelled diurnal variation of HOCl, ClO, HO_2 and HCl for the tropics and three altitudes (35, 45 and 55 km) and a comparison with satellite observations are presented in **paper II**. Figure 4.1 shows as an example the diurnal variation of ClO at 35 km from the model and observations made by ISS/SMILES, Aura/MLS and Odin/SMR.
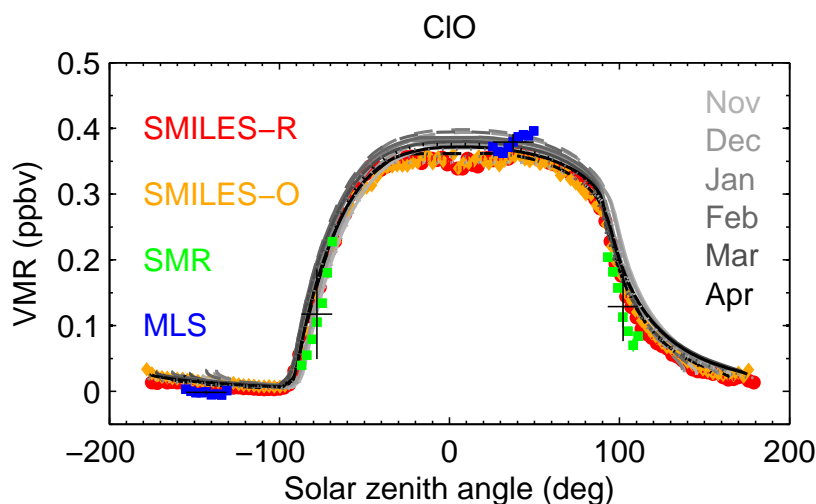
Figure 4.1: Modeled diurnal variation of ClO at 35 km in the tropics compared to observations made by SMILES, Aura/MLS and Odin/SMR during the period November 2009 to April 2010. SMILES data are presented by two products; the research product (SMILES-R) and the official product (SMILES-O). Model simulations represent different months from November (light gray) to April (dark gray).

The model has been run at three latitudes (20°N, 0° and 20°S) and six representative months (November to April, the period of SMILES observations) to provide simulations for comparison with satellite measurements of ClO, HOCl and HO_2. The temper-

ature and pressure profiles used in the model were taken from analyses of the European Center for Medium-Range Weather Forecast (ECMWF). The model uses output from the Canadian Middle Atmosphere Model (CMAM) for initialization of the trace gas profiles at noontime (local solar time of 12). The total inorganic chlorine, which comprises the sum of [ClO], 2[Cl$_2$O$_2$], [HCl], [ClONO$_2$], [Cl], [OClO], [BrCl], [HOCl] and [Cl$_2$], is constrained according to the study by Nassar et al. [2006] based on ACE-FTS and Odin/SMR observations in the tropical stratosphere. We initialize the model HCl profile with the Cl$_y$ (as HCl is the main chlorine reservoir) and let the model calculate the partitioning of chlorine families based on the chemical schemes and reaction rates. The concentration of radicals is initially set to zero. These species are formed in the model by chemical reactions. The water profile is initialized according to the average of measured profiles by Aura/MLS between 20°N and 20°S for the period of SMILES observations (October 2009-April 2010).

For the sake of completeness and to give an overview, the partitioning of chlorine, bromine, nitrogen, hydrogen and oxygen compounds in the tropical stratosphere and lower mesosphere are shown in this chapter.

4.1 Model results

In this section the model results for partitioning of the chemical species within their respective families are presented. The plots show the day and night profiles of chemical species between 20–55 km and the diurnal variation of species versus local solar time. More details on the model comparison with observations are presented in **paper II**.

4.1.1 Chlorine species

Figure 4.2 shows the vertical distribution of chlorine species at the equator for solar condition of 1 November from 20 to 55 km in linear and logarithmic scales. The logarithmic plot visualizes the profiles for minor species. Profiles are plotted for noon and midnight and comprise the lower stratosphere to the lower mesosphere region. Figure 4.2 shows that HCl is clearly the largest contributor to Cl$_y$ from the stratosphere to the mesosphere. According to WMO [2010] it accounts for more than 95% of the total stratospheric chlorine above 50 km. Secondary contributors are ClO, HOCl and ClONO$_2$ from the lower to the middle stratosphere and ClO and HOCl in the upper stratosphere and the lower mesosphere. HOCl is a temporary reservoir for the reactive chlorine species (mostly nighttime), since it is mainly photolysed (reaction 2.44) and, to a lesser extent, destroyed by the reaction with OH, Cl and atomic oxygen during the day.
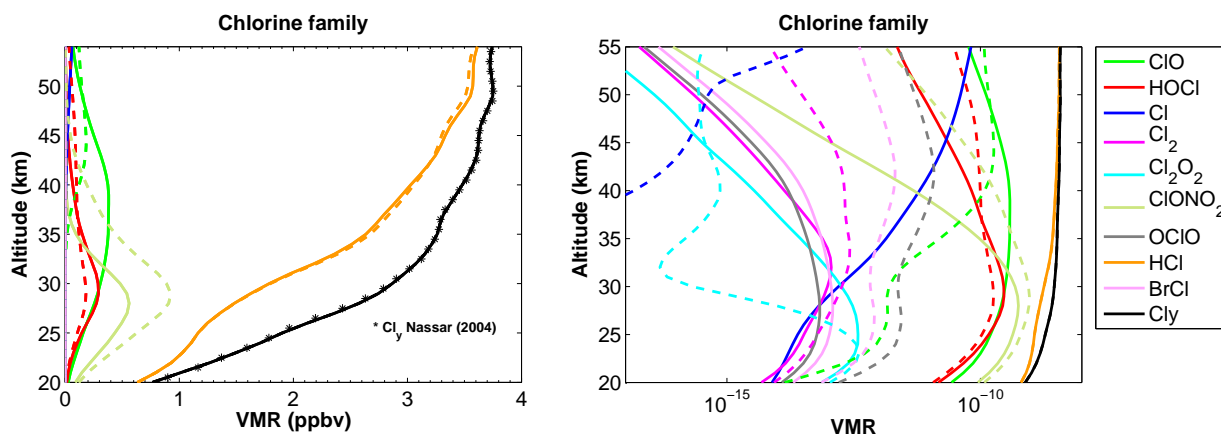
Figure 4.2: Vertical distribution of chlorine species (left: linear scale, right: logarithmic scale), simulated for conditions of 1st of November in the tropics. The total inorganic chlorine in the model is constrained according to measurements by ACE-FTS and Odin/SMR from 30°–30° (Nassar et al. [2006]). Profiles of the model species at noon are shown as solid lines and profiles at midnight as dashed lines.

$$
\begin{aligned}
HOCl + O &\rightarrow OH + ClO & (4.1) \\
HOCl + Cl &\rightarrow HCl + ClO & (4.2) \\
HOCl + OH &\rightarrow H_2O + ClO & (4.3)
\end{aligned}
$$

Photolysis of HOCl is most significant above 45 km as seen in Figure 4.2. The HOCl maximum is located at about 25-30 km and is formed mostly by the reaction of ClO with HO_2 radicals (reaction 2.39). The formation via OH reactions with $ClONO_2$ and Cl_2 are of minor significance:

$$
\begin{aligned}
OH + ClONO_2 &\rightarrow HOCl + NO_3 & (4.4) \\
OH + Cl_2 &\rightarrow HOCl + Cl & (4.5)
\end{aligned}
$$

ClO in unperturbed conditions is mostly produced by the reaction of Cl atoms, released from the photolysis of organic chlorine species, and ozone molecules (reaction 2.8). Chlorine monoxide reacts with atomic oxygen which occurs mostly in the upper stratosphere to mesosphere and gives rise to Cl atoms. This can be seen in Figure 4.3 as the sharp rise of chlorine atoms at 45 Km and particularly at 55 km during the day, where the abundance of atomic oxygen is maximum (Figure 4.11).

$$
ClO + O \rightarrow Cl + O_2 \qquad (4.6)
$$

ClO is formed during daytime mainly by the photo-dissociation of $ClONO_2$ in the lower to middle stratosphere region. This leads to an anti-correlation between ClO and $ClONO_2$ at 35 and 45 km. Formation of $ClONO_2$ through reaction of ClO and NO_2 has a significant diurnal variation mostly due to photolysis and reaction with atomic

oxygen. The probability of both reactions increases with altitude. Reaction of OH and HCl converts reservoir chlorine to the active form (Cl). HCl is formed via several reactions, most importantly by the reactions of atomic chlorine with methane or HO_2. HCl has a very small diurnal variation in the altitude range considered in this study. However, due to its relatively long life-time (about one month in the lower stratosphere), transport has some effect on the distribution and diurnal cycle of HCl [Brasseur et al., 1999] and consequently HCl can not fully be simulated by a 1-D model.
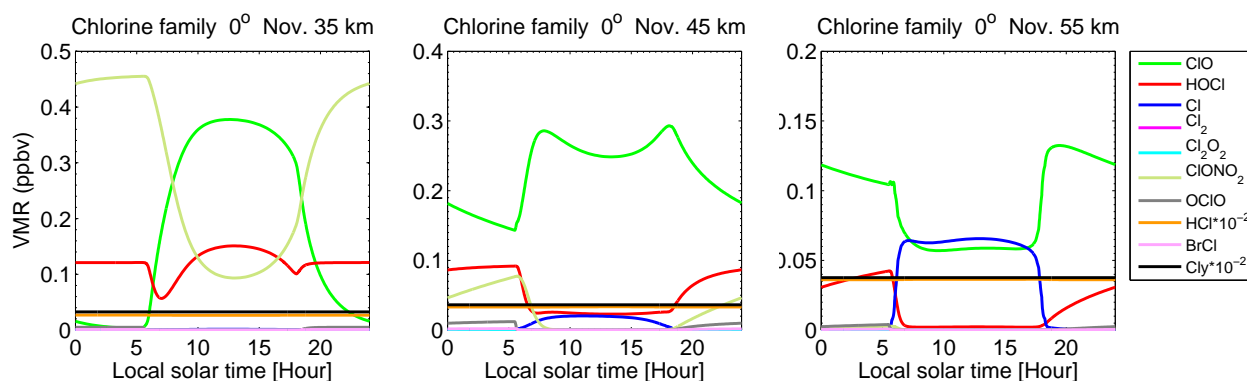
Figure 4.3: Modeled diurnal variation of chlorine species in the tropics (latitude 0°) calculated for November 1 and altitudes of 35, 45 and 55 km (left, middle and right). The diurnal variation of species is presented as volume mixing ratio versus local solar time. HCl and Cl_y have been scaled down for better visualization of minor species (see legend).
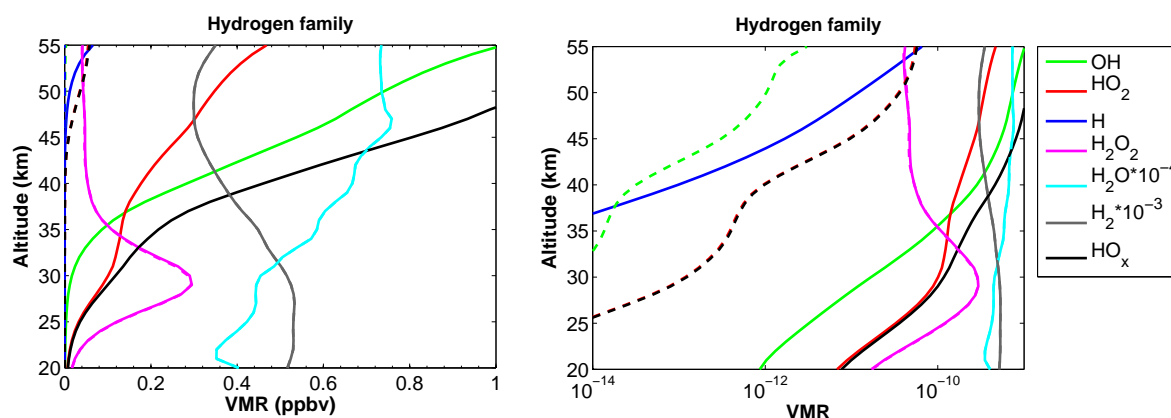
Figure 4.4: Vertical distribution of hydrogen species (left: linear scale , right. logarithmic scale), simulated for conditions of 1st November in the tropics. Water is initialized according to water profiles measured by MLS on 1st November 2009. Temperature and pressure profiles are taken from ECMWF analyses. Profiles of the model species at noon are shown as solid lines and profiles at midnight as dashed lines. The water vapour profile is scaled down for better visualization of other hydrogen family species.
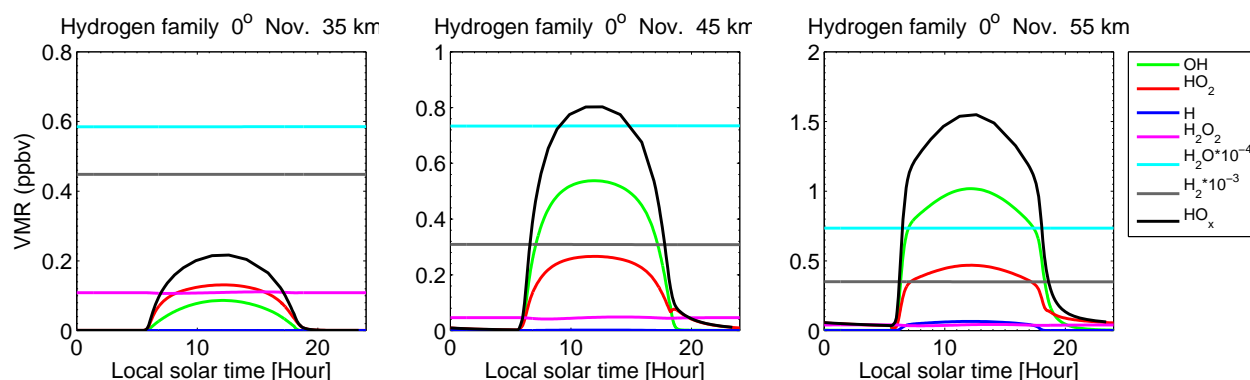
Figure 4.5: Modeled diurnal variation of hydrogen species in the tropics (latitude 0°) calculated for November 1st and altitudes of 35, 45 and 55 km (left, middle and right). The diurnal variation of species is presented as volume mixing ratio versus local solar time. H_2O and H_2 have been scaled down for better visualization of minor species (see legend). HO_x is the sum of OH, HO_2 and H.
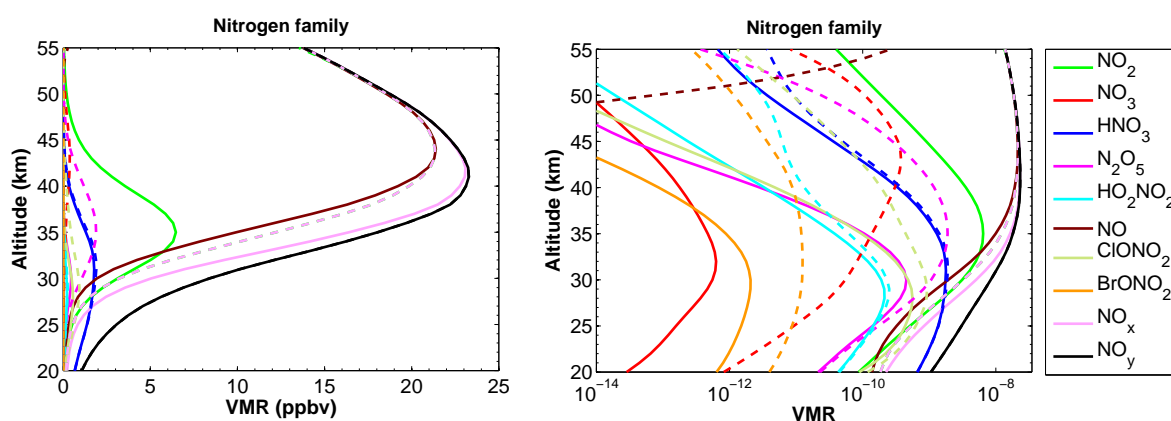
4.1.2 Hydrogen species

Model calculations for the hydrogen family are shown in Figures 4.4 and 4.5. H_2O and H_2 are the main hydrogen species in the stratosphere. The secondary species are OH and HO_2 from 35 to 55 km. Water reaches the stratosphere by ascending air from the tropical troposphere. The stratosphere is dry because water vapor is condensed in the cold tropopause before reaching the stratosphere. The increase of water vapor at altitudes above the middle stratosphere (as shown in Figure 4.4) is the result of methane oxidation and formation of water molecules. Water vapor is not photolyzed in the stratosphere and lower mesosphere regions and therefore has no day-night variation. The sources of OH and HO_2 have been discussed in section 2.2.2. The life-times of OH and HO_2 are very short in the stratosphere and mesosphere and these radicals inter-convert quickly. Their atmospheric abundance is the result of equilibrium between their formation by photo-chemistry and their destruction by recombination, which generates water or by combination with other species. OH and HO_2 are formed to a greater extent at higher altitudes in the stratosphere, where both water and atomic oxygen are more abundant. Hydrogen peroxide, H_2O_2, is formed by self reaction of HO_2 radicals and is photolysed during the day. Between 25 and 35 km, H_2O_2 dominates HO_x ([OH]+[HO_2]+[H]). The abundance of HO_x species in the stratosphere is not affected by transport, due to their short life-time, however transport of the source gas H_2O will effect HO_x indirectly.

4.1.3 Nitrogen species

Model calculation of NO_y family (sum of HNO_3, NO, NO_2, NO_3, $ClONO_2$, $BrONO_2$, N_2O_5 and HO_2NO_2) are shown in Figures 4.6 and 4.7. NO and NO_2 are very reactive species which inter-convert quickly and together with HNO_3 comprise most of the total nitrogen species (NO_y). This is shown in Figure 4.6 as the NO_x profile

(NO+NO$_2$+NO$_3$) is very close to the NO$_y$ profile above 30 km as HNO$_3$ decreases with altitude. NO$_x$ species have a significant diurnal variation, as a result of photolysis reactions as well as the reaction with atomic oxygen or peroxy radicals (HO$_2$). NO$_2$ is more abundant in nighttime, while NO is more abundant during daytime. N$_2$O$_5$ and NO$_3$ which are formed at nighttime are photo-dissociated during the day and give NO and NO$_2$. The photolysis of N$_2$O$_5$ is slow, but NO$_3$ is photolysed quickly. This can be seen in Figure 4.7 as the slower decrease of N$_2$O$_5$ and a sharp drop of NO$_3$ after sunrise. HNO$_3$, ClONO$_2$, BrONO$_2$ and HO$_2$NO$_2$ are reservoirs of odd nitrogen and are formed through reactions with radicals of the chlorine, bromine and hydrogen species. These reservoirs temporarily restrict the amount of radicals available for ozone destruction cycles.
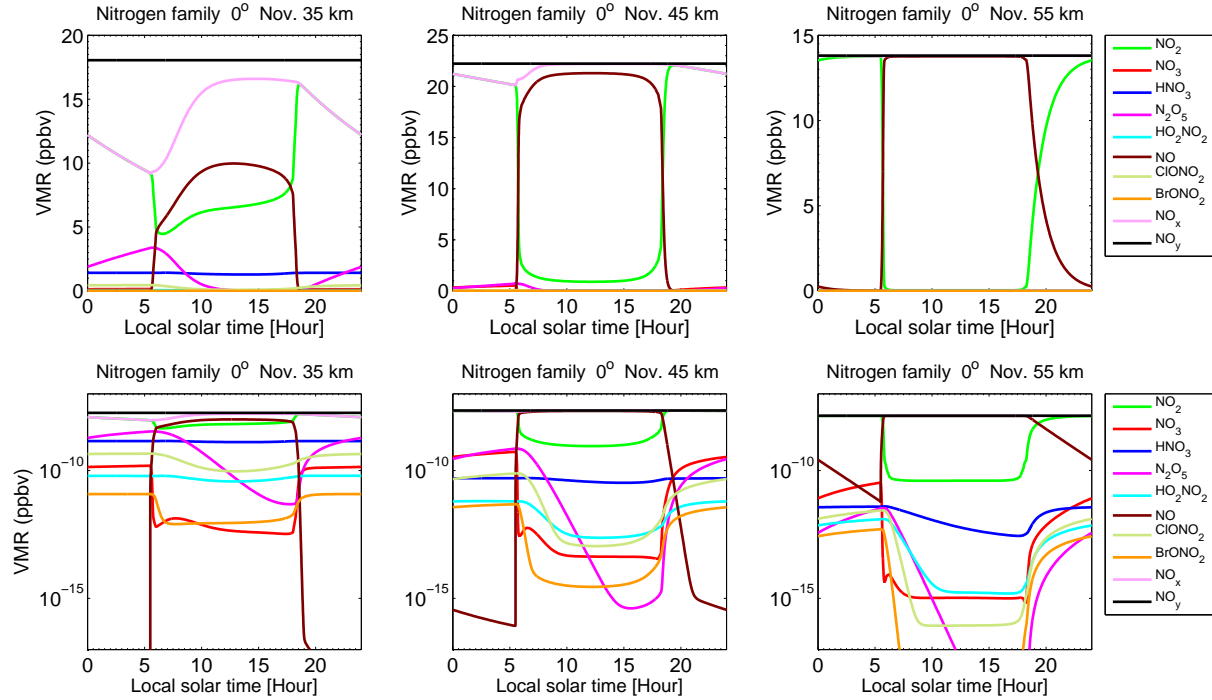

Figure 4.6: Vertical distribution of nitrogen species (left: linear scale, right: logarithmic scale), simulated for conditions of 1st November in the tropics. Profiles at noon and midnight are shown as solid and dashed lines, respectively. NO$_x$ midnight profile overlaps NO$_2$ midnight profile.
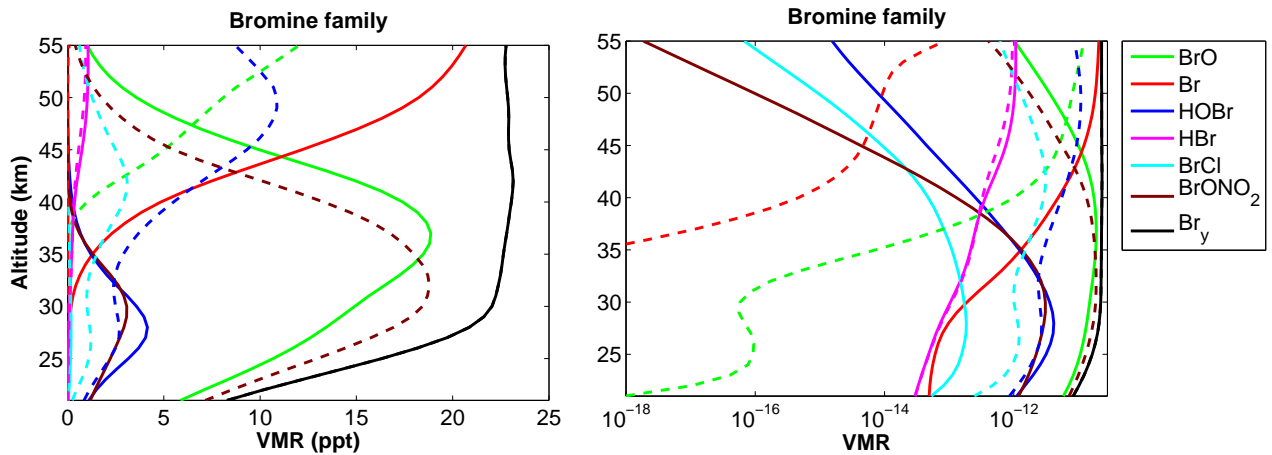
4.1.4 Bromine species

Bromine species are shown in Figure 4.8 and 4.8. BrO is the main contributor to the total inorganic bromine, Br$_y$ (Br$_y$=Br+BrO+HBr+HOBr+BrONO$_2$+BrCl), during daytime and below about 40 km. HBr and BrONO$_2$ are the secondary and tertiary daytime species in the lower stratosphere at approximately 20–30 km. At altitudes above, Br is the most dominant species due to photolysis of BrO and other bromine species or their reactions with atomic oxygen at higher levels. During the night, Br$_y$ is made up of BrONO$_2$ below about 40 km and HOBr and BrO around 50 km. All bromine reservoirs (BrONO$_2$, HOBr and HBr) are photolysed and unstable during the day.

The diurnal variation of bromine species is illustrated in Figure 4.9. The chemistry of bromine species is similar to that of chlorine species. In the gas phase, BrO is mainly formed by the reaction of Br and ozone. Below $\sim$40 km, BrO is the most abundant inorganic bromine species during daytime and BrONO$_2$ is the most abundant species

Figure 4.7: Modeled diurnal variation of nitrogen species in the tropics (latitude 0°) calculated for November 1 and altitudes of 35, 45 and 55 km (left, middle and right). Top: linear, bottom: logarithmic y-axis. The diurnal variation is presented as volume mixing ratio versus local solar time. Here, NO_x is defined as the sum of NO and NO_2.

Figure 4.8: Vertical distribution of bromine species (left: linear scale, right: logarithmic scale), simulated for conditions of 1st November in the tropics. Profiles at noon and midnight are shown as solid and dashed lines, respectively.

at nighttime. Photo-dissociation of $BrONO_2$ leads to the formation of daytime BrO mostly at 35 and 45 km. The $BrONO_2$ contribution to the peak of daytime BrO decreases above 35 km. $BrONO_2$ at night is formed by reaction of BrO with NO_2 radicals. At 55 km, BrO concentrations drop during daytime mainly due to the reaction with

51
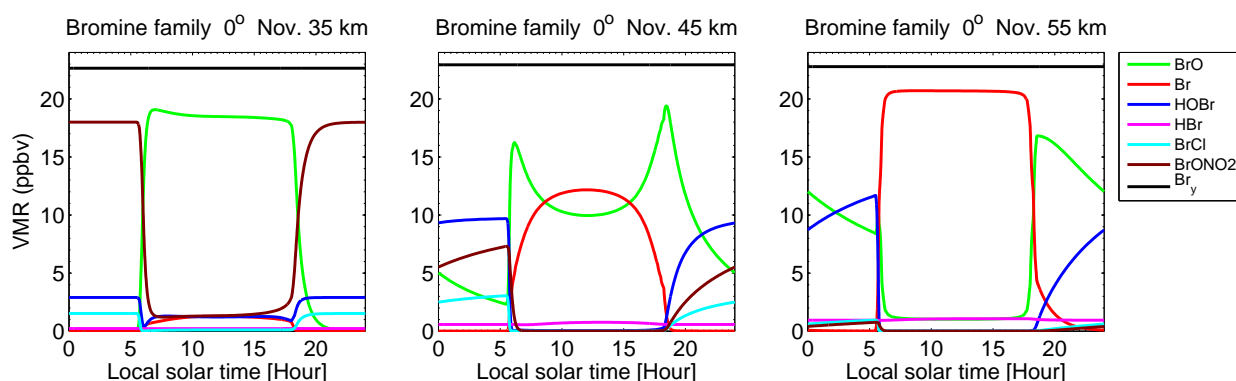
Figure 4.9: Modeled diurnal variation of bromine species in the tropics (latitude 0°) calculated for November 1 and altitudes of 35, 45 and 55 km (left, middle and right). The diurnal variation of species is presented as volume mixing ratio versus local solar time.

atomic oxygen which gives rise to bromine atoms. At 45 km, the shape of BrO during the day is interesting, as the photolysis of $BrONO_2$ gives rise to sunrise values, but BrO reaction with atomic oxygen lowers the peak of BrO. BrCl and HOBr photolysis occurs in the lower stratosphere below about 25-30 km and the main loss above these altitudes is attributed to the reaction with atomic oxygen which leads to the formation of Br [Brasseur et al., 1999, Brasseur and Solomon, 2005].

4.1.5 Oxygen species

Figure 4.10 shows the vertical profile for oxygen species in the MISU-1D model. As the Figure shows, the maximum peak of ozone is located around 30 km in the equatorial stratosphere and ozone is the main constituent of odd oxygen (O_x) between 20 to 55 km. Ozone decreases towards mesospheric altitudes, but atomic oxygen increases. Transport plays an important role on the abundance of ozone (and O_x) in the atmosphere, as has been discussed in section 2.2.1. The reactions converting ozone, oxygen molecules and atoms have also been described in section 2.2.1.

The diurnal variation of oxygen compounds in the tropics at the altitudes of 35, 45 and 55 km are shown in Figure 4.11. These changes are not visible for atomic oxygen in linear scale (top row of Figure 4.11), but are better visualized in logarithmic scale (bottom row). At stratospheric and mesospheric altitudes atomic oxygen exhibits a very distinct day-to-night variation. Its stratospheric concentration drops quickly after sunset and is converted to ozone molecules (reaction 2.5). Ozone has a shorter life-time toward higher altitudes (above ∼45 km) and shows larger diurnal variability. Atomic oxygen has an opposite behavior and longer life-time at higher altitudes [Brasseur and Solomon, 2005].
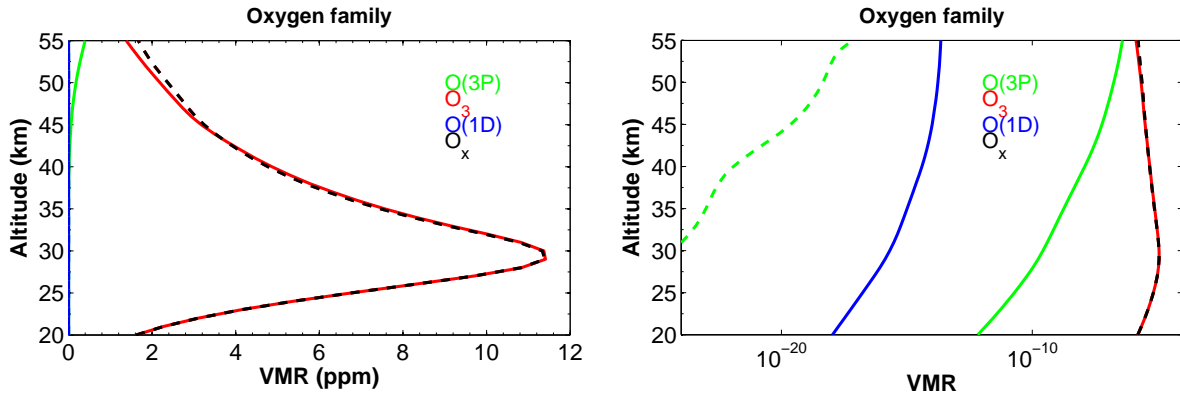
Figure 4.10: Vertical distribution of oxygen compounds (left: linear scale, right: logarithmic scale) simulated for conditions of 1st November in the tropics. O_x represents the sum of and $O(^1D)$, $O(^3P)$ and O_3. Profiles at noon and midnight are shown as solid and dashed lines, respectively, except for O_x during daytime which is plotted as dashed line for better visibility as it overlaps with the O_3 profile. O_x profile for the night is not plotted here, since it overlaps the daytime O_x at altitudes below 45 km and O_3 above 45 km.
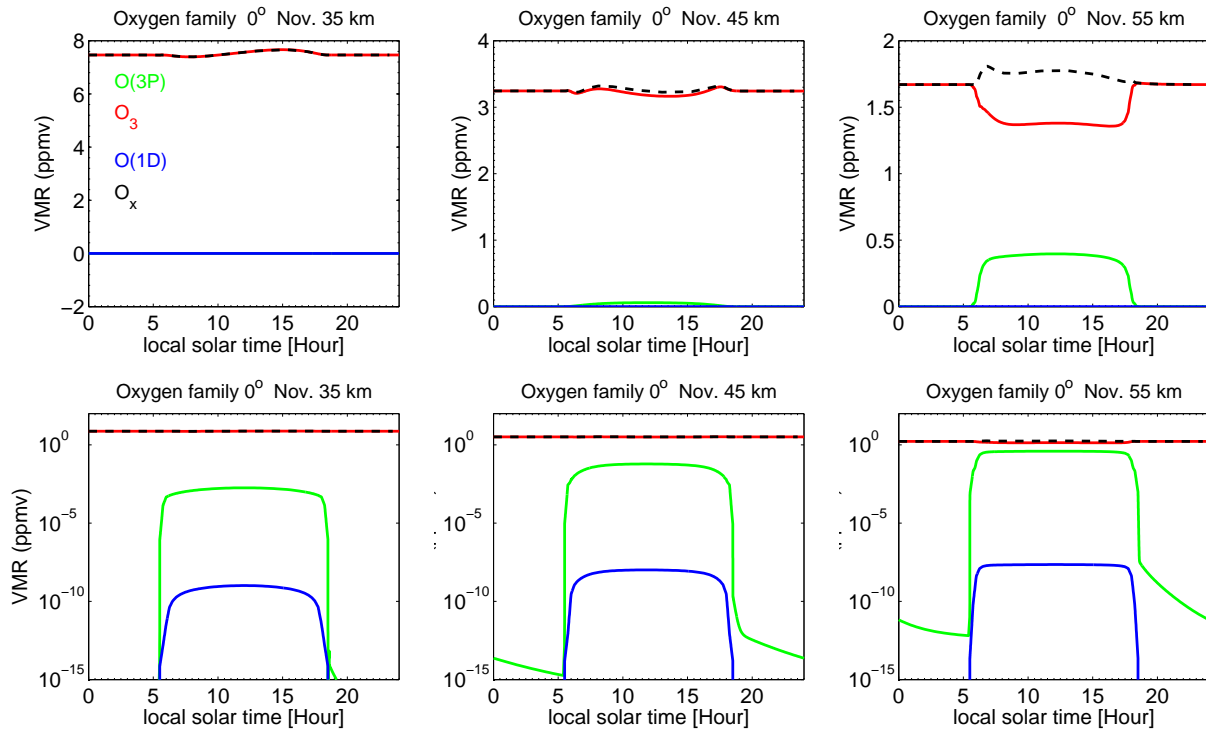
Figure 4.11: Modeled diurnal variation of oxygen compounds in the tropics (latitude 0°) calculated for November 1 and altitudes of 35, 45 and 55 km (left, middle and right). The diurnal variation of species is presented as volume mixing ratio versus local solar time. O_x represents the sum of and $O(^1D)$, $O(^3P)$ and O_3. The plots in the bottom row are plotted in logarithmic scale for better visualization of $O(^1D)$ and $O(^3P)$.

53

Chapter 5

Summary and Conclusions

In this work a brief introduction to atmospheric physics and chemistry of stratospheric ozone and related species is given. Emphasis is placed on photo-chemical modeling of the Arctic lower stratosphere and the tropical stratosphere and lower mesosphere regions. The model results are compared to observations. The thesis is based on two papers. Paper I, describes the modelled ClO diurnal variation in the Arctic winter lower stratosphere and compares the results with observations by ASUR (Airborne SUbmillimeter Radiometer) measurements from three years (1996, 1997 and 2000). Paper II compares the model diurnal variation of the short-lived species HOCl, ClO and HO_2 (as well as HCl as the main chlorine reservoir) in the tropical middle stratosphere to lower mesosphere region with satellite observations.

5.1   Summary of paper I

Measurements of the lower stratospheric ClO across the terminator taken by the Airborne SUb-millimeter Radiometer (ASUR) in the activated polar vortices of the Arctic winters of 1995-96, 1996-97 and 1999-2000 are analyzed to evaluate the plausibility of ClO-dimer photolysis cross-sections and the rate constants controlling the thermal equilibrium between the ClO-dimer and ClO published in recent literature. Measured ClO at low solar zenith angles is used to estimate the total active chlorine (ClO_x). ClO_x estimates based on different photolysis rates of the ClO-dimer are compared with total available inorganic chlorine (Cl_y). Cl_y is estimated from a N_2O and Cl_y correlation established by a balloon measurement of the MarkIV interferometer in December 1999. The results show that cross-sections leading to the fastest photolysis rates in literature give ClO_x mixing ratios that overlap with the estimated range of available Cl_y. Slower photolysis rates lead to ClO_x values that are increasingly higher than the available Cl_y.

We further used the calculated ClO from low solar zenith angles to estimate ClO in darkness based on different equilibrium constants, and compared it with ASUR ClO measurements before sunrise at high solar zenith angles. It was found that calculations with equilibrium constants published in the kinetics evaluations of the Jet Propulsion Laboratory of recent years give good agreement with observed ClO mixing

ratios within the combined uncertainties of this study. Equilibrium constants leading to a higher ClO/ClO_x ratio in darkness yield ClO values that exceed the ones observed.

Additionally several sensitivity tests have been performed to support the results in the paper. The model sensitivity to the temperature and albedo uncertainties has been tested. The effect of inclusion of the ClO-BrO cycle besides the ClO-dimer cycle on the ClO diurnal variation has also been examined.

5.2   Summary of paper II

The diurnal variation of hypochlorous acid (HOCl) and the related species chlorine monoxide (ClO), hydroperoxyl (HO_2) as well as hydrogen chloride (HCl) as observed by satellite instruments (Aura/MLS, Odin/SMR, ISS/SMILES, ENVISAT/MIPAS and SCISAT/ACE-FTS) is compared with one-dimensional model calculations (MISU-1D). The satellite data were averaged for the latitude band of 20^oN – 20^oS for the SMILES period of observations from November 2009 to April 2010. The average water profile from Aura/MLS for the same period and location is used to initialize the model. The total inorganic chlorine is constrained according to Nassar et al. [2006] and temperature and pressure are taken from ECMWF analyses. HOCl as a temporary chlorine reservoir is mainly formed by the reaction of HO_2 with ClO and its abundance is controlled by photo-chemistry. The diurnal variation of these species was compared at three levels (35, 45 and 55 km). The paper also presents a first evaluation of Odin/SMR HO_2 measurements and the first comparison of the new SMILES data with the latest versions of other satellite data sets.

The model diurnal cycles were assessed by comparison with the satellite observations. In particular, SMILES is the only instrument performing measurements over all solar zenith angles and enables us to have a full observational picture of the diurnal variation of these species. For this purpose, the model has been run for solar conditions of three latitudes 20^oN, 0° and 20^oS and six representative months (November to April). The model results were smoothed using 5 and 7 km moving averages for 35 km and the levels above, respectively, to account for the limited altitude resolution of the measurements. The results of the comparisons indicate a reasonably good agreement between the model and observations in terms of the characteristical shape of the diurnal variations, the absolute values as well as the amplitudes of the day and night variations.

Bibliography

L. M. Avallone and D. W. Toohey. Tests of halogen photochemistry using in situ measurements of ClO and BrO in the lower polar stratosphere. *J. Geophys. Res.*, 106(D10): 10411–10, 2001.

G. Berthet, P. Ricaud, F. Lefèvre, E. Le Flochmoën, J. Urban, B. Barret, N. Lautié, E. Dupuy, J. De La Noë, and D. Murtagh. Nighttime chlorine monoxide observations by the odin satellite and implications for the ClO/Cl_2O_2 equilibrium. *Geophysical Research Letters*, 32(11):L11812, 2005.

G. P. Brasseur and S. Solomon. *Aeronomy of the Middle Atmosphere*. Springer, Dordrecht, The Netherlands, 3rd edition, 2005.

G. P. Brasseur, J. J. Orlando, and G. S. Tyndall. *Atmospheric Chemistry and Global Change*. Oxford University Press, New York, Oxford, 1999.

J. B. Burkholder, J. J. Orlando, and C. J. Howard. Ultraviolet absorption cross sections of Cl_2O_2 between 210 and 410 nm. *J.Phys.Chem.*, 94:687–695, 1990.

H. Y. Chen, C. Y. Lien, W. Y. Lin, Y. T. Lee, and J. J. Lin. UV absorption cross sections of ClOOCl are consistent with ozone degradation models. *Science*, 324(5928):781, 2009.

M. P. Chipperfield, W. Feng, and M. Rex. Arctic ozone loss and climate sensitivity: Updated three-dimensional model study. *Geophys. Res. Lett.*, 32(11), 2005.

B. J. Connor, T. Mooney, J. Barrett, P. Solomon, A. Parrish, and M. L. Santee. Comparison of ClO measurements from the Aura Microwave Limb Sounder to ground-based microwave measurements at Scott Base, Antarctica, in spring 2005. *J. Geophys. Res*, 112, 2007.

R. A. Cox and G. D. Hayman. The stability and photochemistry of dimers of the ClO radical and implications for Antarctic ozone depletion. *Nature*, 332(28), 1988.

Veronika Eyring. *Model studies on the Arctic stratospheric chemistry compared to measurements*. PhD thesis, University of Bremen, 1999. Reports on Polar Research, No. 320, ISSN 0176-5027.

J. C. Farman, B. D. Gardiner, and J. D. Shanklin. Large losses of total ozone in Antarctica reveal seasonal ClO_x/NO_x interaction. *Nature*, 315:207–210, 1985. doi: 10.1038/ 315207a0.

B. J. Finlayson-Pitts and J. N. Pitts. *Chemistry of the Upper and Lower Atmosphere*. Academic Press, 1st edition, 1999. ISBN 0-12-257060-x.

K. Frieler, M. Rex, R. J. Salawitch, T. Canty, M. Streibel, R. M. Stimpfle, K. Pfeilsticker, M. Dorf, D. K. Weisenstein, S. Godin-Beekmann, et al. Toward a better quantitative understanding of polar stratospheric ozone loss. *Geophys. Res. Lett*, 33(10), 2006.

R. R. Garcia and S. Solomon. A new numerical model of the middle atmosphere 2. Ozone and related species. *J. Geophys. Res.*, 99:12937–12951, 1994.

K. J. Huder and W. B. DeMore. Absorption cross-sections of the ClO dimer. *J. Phys. Chem*, 99:3905–3908, 1995.

A. Jones, J. Urban, D. P. Murtagh, C. Sanchez, K. A. Walker, L. Livesey, L. Froidevaux, and M. L. Santee. Analysis of HCl and ClO time series in the upper stratosphere using satellite data sets. *Atmos. Chem. Phys.*, 11:5321–5333, 2011.

A. Jonsson. Studier av ozon i övre stratosfären och lägre mesosfären med hjälp av satellitdata. Master's thesis, Stockholm University, November 1996. TRITA-FYS 5237.

A. Jonsson. *Modelling the middle atmosphere and its sensitivity to climate change*. PhD thesis, Stockholm University, 2006.

R. Kivi, E. Kyrö, T. Turunen, N. R. P. Harris, P. von der Gathen, M. Rex, S. B. Andersen, and I. Wohltmann. Ozonesonde observations in the Arctic during 1989–2003: Ozone variability and trends in the lower stratosphere and free troposphere. *J. Geophys. Res.*, 112, 2007. doi: 10.1029/2006JD007271.

Armin Kleinböhl. *Airborne submillimeter measurements of Arctic middle atmospheric trace gases*. PhD thesis, University of Bremen, 2004.

G. A. Koppers and D. P. Murtagh. Model studies of the influence of O_2 photodissociation parametrizations in the Schumann-Runge bands on ozone related photolysis on the upper atmosphere. *Annales Geophysicae*, 14:68–79, 1996.

M. J. Kurylo, B-M. Sinnhuber, N. R. P. Harris, M. von Hobe, P. A. Newman, D. W. Fahey, R.S. Gao, R. J. Salawitch, M. P. Chipperfield, J. G. Anderson, M. L. Santee, T. P. Canty, R. Müller, R. Schofield, R. M. Stimpfle, F. Stroh, D. W. Toohey, J. Urban, S. R. Kawa, D. J. Hofmann, K. W. Hoppel, M. Rex, K. D. Bayes, D. A. Dixon, K. W. Jucks, S. P. Sander, J. U. Grooß, and D. E. Kinnison. The role of halogen chemistry in polar stratospheric ozone depletion. Technical report, Report from the June 2008 Cambridge, UK Workshop for an Initiative under the Stratospheric Processes and Their Role in Climate (SPARC) Project of the World Climate Research Program, 2009.

D. J. Lary and J. A. Pyle. Diffuse radiation, twilight, and photochemistry-I. *J. Atmos. Chem.*, 13:373–392, 1991.

C. Y. Lien, W. Y. Lin, H. Y. Chen, W. T. Huang, B. Jin, I. C. Chen, and J. J. Lin. Photodissociation cross sections of ClOOCl at 248.4 and $266\ nm$. *J. Chem. Phys.*, 131:174301, 2009.

S. Madronich. *The atmosphere and UV-B radiation at ground level, in Environmental UV Photobiology*. L.O. Bjorn and A.R. Young eds., 1993.

G. L. Manney, M. L. Santee, M. Rex, N. J. Livesey, M. C. Pitts, P. Veefkind, E. R. Nash, I. Wohltmann, R. Lehmann, L. Froidevaux, L. R. Poole, R. Lamont, M. R. Schoeberl, D. P. Haffner, J. Davies, V. Dorokhov, H. Gernandt, B. Johnson, R. Kivi, E. Kyro, N. Larsen, P. F. Levelt, A. Makshtas, C. T. McElroy, H. Nakajima, M. C. Parrondo, D. W. Tarasick, P. von der Gathen, K. A. Walker, and N. S. Zinoviev. Unprecedented Arctic ozone loss in 2011. *Nature*, 478:469–475, 2011. doi: 10.1038/nature10556.

M. B. McElroy, R. J. Salawitch, S. C. Wofsy, and J. A. Logan. Reductions of Antarctic ozone due to synergistic interactions of chlorine and bromine. *Nature*, 321:759–762, 1986. doi: 10.1038/321759a0.

C.A. McLinden, C.S. Haley, N.D. Lloyd, F. Hendrick, A. Rozanov, B. M. Sinnhuber, F. Goutail, D.A. Degenstein, E.J. Llewellyn, C.E. Sioris, M. Van Roozendael, J.P. Pommereau, M. Lotz, and J.P. Burrows. Odin/OSIRIS observations of stratospheric BrO: Retrieval methodology, climatology, and inferred Br_y. *J. Geophys. Res.*, 115:D15308, 2010. doi: 10.1029/2009JD012488.

R. R. Meier, D. E. jr. Anderson, and M. Nicolet. Radiation field in the troposphere and stratosphere from $240 − −1000nm − I$. General analysis. *Planetary and Space Science*, 30(9):923–933, 1982. ISSN 0032–0633. doi: 10.1016/0032-0633(82)90134-9.

L. T. Molina and M. J. Molina. Production of chlorine oxide (Cl_2O_2) from the self-reaction of the chlorine oxide (ClO) radical. *J. Phys. Chem.*, 91(2):433–436, 1987. doi: 10.1021/j100286a035.

R. Nassar, P. F. Bernath, C. D. Boone, C. Clerbaux, P. F. Coheur, G. Dufour, L. Froidevaux, E. Mahieu, J. C. McConnell, S.D. McLeod, D. P. Murtagh, C. P. Rinsland, K. Semeniuk, R. Skelton, K. A. Walker, and R. Zander. A global inventory of stratospheric chlorine in 2004. *J. Geophys. Res*, 111:D22312, 2006.

S. L. Nickolaisen, R. R. Friedl, and S. P. Sander. Kinetics and mechanism of the ClO+ClO reaction - pressure and temperature dependences of the bimolecular and termolecular channels and thermal-decomposition of chlorine peroxide. *J. Phys. Chem.*, 98:155–169, 1994.

M. Nicolet and R. Kennes. Aeronomic problems of the molecular oxygen photodissociation-I. The O_2 Herzberg continuum. *Planet*, 34:1043, 1986.

D. K. Papanastasiou, V. C. Papadimitriou, D. W. Fahey, and J. B. Burkholder. UV absorption spectrum of the ClO Dimer (Cl_2O_2) between 200 and $420\ nm$. *J. Phys. Chem. A*, 113(49):13711–13726, 2009.

T. Permien, R. Vogt, and R. N. Schindler. *Absorption spectra of HOCl and Cl₂O₂, in Mechanisms of Gas Phase-Liquid Phase Chemical Transformations*. Number Air Pollution Report no.17. Environmental Research Program of the CEC, Brussels, Belgium, 1988.

K. Pfeilsticker, W. T. Sturges, H. Bösch, C. Camy-Peyret, M. P. Chipperfield, A. Engel, R. Fitzenberger, M. Müller, S. Payan, and B. Sinnhuber. Lower stratospheric organic and inorganic bromine budget for the Arctic winter 1998/99. *Geophys. Res. Lett.*, 27 (20):3305–3308, 2000.

J. Plenge, S. Kuhl, B. Vogel, R. Müller, F. Stroh, M. von Hobe, R. Flesch, and E. Rühl. Bond strength of chlorine peroxide. *J. Phys. Chem. A*, 109(30):6730–6734, 2005.

F. D. Pope, J. C. Hansen, D. Kyle, R. R. Friedl, and S. P. Sander. Ultraviolet absorption spectrum of chlorine peroxide, ClOOCl. *J. Phys. Chem. A*, 111(20):4322–4332, 2007.

C. P. Rinsland, E. Mahieu, R. Zander, N. B. Jones, M. P. Chipperfield, A. Goldman, J. Anderson, J. M. Russell III, P. Demoulin, J. Notholt, G. C. Toon, J. F. Blavier, B. Sen, R. Sussmann, S. W. Wood, A. Meier, D. W. T. Griffith, L. S. Chiou, F. J. Murcray, T. M. Stephen, F. Hase, S. Mikuteit, A. Schulz, and T. Blumenstock. Long-term trends of inorganic chlorine from ground-based infrared solar spectra: Past increases and evidence for stabilization. *J. Geophys. Res.*, 108, 2003. doi: 10.1029/2002JD003001.

S. P. Sander, R. R. Friedl, J. R. Barker, , D. M. Golden, M. J. Kurylo, P. H. Wine, J. P. D. Abbatt, J. B. Burkholder, C. E. Kolb, G. K. Moortgat, R. E. Huie, and V. L. Orkin. Chemical kinetics and photochemical data for use in atmospheric studies: supplement to evaluation 12: update of key reactions. Technical report, JPL, 2000. Evaluation number 13, JPL Publ., 00-3.

S. P. Sander, R. R. Friedl, J. R. Barker, , D. M. Golden, M. J. Kurylo, P. H. Wine, J. P. D. Abbatt, J. B. Burkholder, C. E. Kolb, G. K. Moortgat, R. E. Huie, and V. L. Orkin. Chemical kinetics and photochemical data for use in atmospheric studies. Technical report, JPL, 2006. Evaluation number 15, JPL Publ., 06-2.

S. P. Sander, R. R. Friedl, J. R. Barker, , D. M. Golden, M. J. Kurylo, P. H. Wine, J. P. D. Abbatt, J. B. Burkholder, C. E. Kolb, G. K. Moortgat, R. E. Huie, and V. L. Orkin. Chemical kinetics and photochemical data for use in atmospheric studies: supplement to evaluation 15: update of key reactions. Technical report, JPL, 2009. Evaluation number 16, JPL Publ., 09-31.

S. P. Sander, R. R. Friedl, J. R. Barker, , D. M. Golden, J. B. Burkholder, C. E. Kolb, M. J. Kurylo, G. K. Moortgat, P. H. Wine, J. P. D. Abbatt, R. E. Huie, and V. L. Orkin. Chemical kinetics and photochemical data for use in atmospheric studies. Technical report, JPL, 2011. Evaluation number 17, JPL Publ., 10-6.

M. L. Santee, I. A. MacKenzie, G. L. Manney, M. P. Chipperfield, P. F. Bernath, K. A. Walker, C. D. Boone, L. Froidevaux, N. J. Livesey, and J. W. Waters. A study of stratospheric chlorine partitioning based on new satellite measurements and modeling. *J. Geophys. Res*, 113:D12307, 2008.

M. L. Santee, S. P. Sander, N. J. Livesey, and L. Froidevaux. Constraining the chlorine monoxide ClO/chlorine peroxide ClOOCl equilibrium constant from aura microwave limb sounder measurements of nighttime ClO. *Proceedings of the National Academy of Sciences*, 107(15):6588, 2010.

R. Schofield, K. Frieler, I. Wohltmann, M. Rex, M. Von Hobe, F. Stroh, G. Koch, T. Peter, T. Canty, R. Salawitch, et al. Polar stratospheric chlorine kinetics from a self-match flight during SOLVE-II/EUPLEX. *Geophysical Research Letters*, 35(1):L01807, 2008.

L. F. Shampine and M. W. Reichelt. The Matlab ODE suite. *SIAM J. Sci. Comput.*, 18: 1–22, 1997.

P. Solomon, J. Barrett, T. Mooney, B. Connor, A. Parrish, and D. E. Siskind. Rise and decline of active chlorine in the stratosphere. *Geophys. Res. Let.*, 33, 2006.

S. Solomon and R. R. Garcia. On the distributions of long-lived tracers and chlorine species in the middle atmosphere. *J. Geophys. Res.*, 89(D7):11633–11644, 1984. doi: 10.1029/JD089iD07p11633.

R. M. Stimpfle, D. M. Wilmouth, R. J. Salawitch, and J.G. Anderson. First measurements of ClOOCl in the stratosphere: The coupling of ClOOCl and ClO in the Arctic polar vortex. *J. Geophys. Res*, 109, 2004.

O. Sumińska-Ebersoldt, R. Lehmann, T. Wegner, J.-U. Grooß, E. Hösen, R. Weigel, W. Frey, S. Griessbach, V. Mitev, C. Emde, C. M. Volk, S. Borrmann, M. Rex, F. Stroh, and M. von Hobe. ClOOCl photolysis at high solar zenith angles: analysis of the RECONCILE self-match flight. *Atmospheric Chemistry and Physics*, 12(3):1353–1365, 2012.

O. P. Tripathi, S. Godin-Beekmann, F. Lefèvre, M. Marchand, A. Pazmino, A. Hauchecorne, F. Goutail, H. Schlager, C.M. Volk, B. Johnson, et al. High resolution simulation of recent Arctic and Antarctic stratospheric chemical ozone loss compared to observations. *J. Atmos. Chem.*, 55(3):205–226, 2006.

J. Urban. *Measurements of the stratospheric trace gases ClO, HCl, O_3, N_2O, H_2O, and OH using air-borne submm-wave radiometry at 650 and 2500 GHz*. PhD thesis, University of Bremen, 1998. Reports on Polar Research, No. 264, ISSN 0176-5027.

J. Urban, K. Sagi, D. Murtagh, and the Odin/SMR team. Evolution of the Arctic lower stratosphere during winter 2010-2011 as observed by the Odin Sub-Millimetre Radiometer. Technical report, Department of Earth and Space Sciences, Chalmers University of Technology, 2011. Odin Arctic winter report 2010/2011, http://www.rss.chalmers.se/~jo/SMRquicklook/Arctic-winter-2011-report/Odin-NH2011- report.pdf.

M. von Hobe, J. U. Grooß, R. Müller, S. Hrechanyy, U. Winkler, and F. Stroh. A re-evaluation of the ClO/Cl_2O_2 equilibrium constant based on stratospheric in-situ observations. *Atmos. Chem. Phys.*, 5(3):693–702, 2005.

M. von Hobe, R. J. Salawitch, T. Canty, H. Keller-Rudek, G. K. Moortgat, J. U. Grooß, R. Müller, and F. Stroh. Understanding the kinetics of the ClO dimer cycle. *ACP*, 7 (12):3055–3069, 2007.

M. von Hobe, F. Stroh, H. Beckers, T. Benter, and H. Willner. The UV/Vis absorption spectrum of matrix-isolated dichlorine peroxide, ClOOCl. *Physical Chemistry Chemical Physics*, 11(10):1571–1580, 2009.

M. von König. *Chlorine activation and PSC formation in the Arctic stratosphere*. PhD thesis, University of Bremen, 2001.

J. M. Wallace and P. V. Hobbs. *Atmospheric Science*. Elsevier Inc., 2nd edition, 2006.

R. P. Wayne. *Chemistry of Atmospheres*. Oxford university press, Third edition, 2000.

P. O. Wennberg, R. C. Cohen, R. M. Stimpfle, J. P. Koplow, J. G. Anderson, R. J. Salawitch, D. W. Fahey, E. L. Woodbridge, E. R. Keim, R. S. Gao, C. R. Webster, R. D. May, D. W. Toohey, L. M. Avallone, M. H. Proffitt, M. Loewenstein, J. R. Podoiske, K. R. Chan, and S. C. Wofsy. Removal of Stratospheric O_3 by Radicals: In Situ Measurements of OH, HO_2, NO, NO_2, CI0, and BrO. *Science*, 266:398–404, 1994.

G. Wetzel, H. Oelhaf, O. Kirner, F. Friedl-Vallon, R. Ruhnke, A. Ebersoldt, A. Kleinert, G. Maucher, H. Nordmeyer, and J. Orphal. Diurnal variations of reactive chlorine and nitrogen oxides observed by MIPAS-B inside the January 2010 Arctic vortex. *Atmospheric Chemistry and Physics*, 12(14):6581–6592, 2012. doi: 10.5194/acp-12-6581-2012. URL http://www.atmos-chem-phys.net/12/6581/2012/.

D. M. Wilmouth, T. F. Hanisco, R. M. Stimpfle, and J. G. Anderson. Chlorine-catalyzed ozone destruction: Cl atom production from ClOOCl photolysis. *J. Phys. Chem. A*, 113(51):14099–14108, 2009.

WMO. Atmospheric Ozone 1985, WMO Global Ozone Research and Monitoring Project, Report No. 16, Geneva, 1986.

WMO. Scientific Assesment of Ozone Depletion 2010, WMO Global Ozone Research and Monitoring Project, Report No. 16, Geneva, 2010.